Lipid Droplet-Associated Proteins (LDAPs) Are Required for the Dynamic Regulation of Neutral Lipid Compartmentation in Plant Cells[1]

Satinder K. Gidda, Sunjung Park, Michal Pyc, Olga Yurchenko, Yingqi Cai, Peng Wu, David W. Andrews, Kent D. Chapman, John M. Dyer*, and Robert T. Mullen*

Department of Molecular and Cellular Biology, University of Guelph, Guelph, Ontario, Canada N1G 2W1 (S.K.G., M.P., R.T.M.); United States Department of Agriculture, Agricultural Research Service, United States Arid-Land Agricultural Research Center, Maricopa, Arizona 85138 (S.P., O.Y., J.M.D.); Department of Biological Sciences, Center for Plant Lipid Research, University of North Texas, Denton, Texas 76203 (Y.C., K.D.C.); and Sunnybrook Research Institute and Department of Biochemistry, University of Toronto, Toronto, Ontario, Canada M4N 3M5 (P.W., D.W.A.)

ORCID IDs: 0000-0002-4722-0006 (S.K.G.); 0000-0001-8702-1661 (M.P.); 0000-0002-8628-7190 (O.Y.); 0000-0002-0357-5809 (Y.C.); 0000-0002-9266-7157 (D.W.A.); 0000-0003-0489-3072 (K.D.C.); 0000-0001-6215-0053 (J.M.D.); 0000-0002-6915-7407 (R.T.M.).

Eukaryotic cells compartmentalize neutral lipids into organelles called lipid droplets (LDs), and while much is known about the role of LDs in storing triacylglycerols in seeds, their biogenesis and function in nonseed tissues are poorly understood. Recently, we identified a class of plant-specific, lipid droplet-associated proteins (LDAPs) that are abundant components of LDs in nonseed cell types. Here, we characterized the three LDAPs in Arabidopsis (*Arabidopsis thaliana*) to gain insight to their targeting, assembly, and influence on LD function and dynamics. While all three LDAPs targeted specifically to the LD surface, truncation analysis of LDAP3 revealed that essentially the entire protein was required for LD localization. The association of LDAP3 with LDs was detergent sensitive, but the protein bound with similar affinity to synthetic liposomes of various phospholipid compositions, suggesting that other factors contributed to targeting specificity. Investigation of LD dynamics in leaves revealed that LD abundance was modulated during the diurnal cycle, and characterization of *LDAP* misexpression mutants indicated that all three LDAPs were important for this process. LD abundance was increased significantly during abiotic stress, and characterization of mutant lines revealed that LDAP1 and LDAP3 were required for the proper induction of LDs during heat and cold temperature stress, respectively. Furthermore, LDAP1 was required for proper neutral lipid compartmentalization and triacylglycerol degradation during postgerminative growth. Taken together, these studies reveal that LDAPs are required for the maintenance and regulation of LDs in plant cells and perform nonredundant functions in various physiological contexts, including stress response and postgerminative growth.

Hydrophobic storage lipids such as triacylglycerols (TAGs) and steryl esters are commonly maintained in the aqueous milieu of the cell's cytoplasm by compartmentalization in lipid droplets (LDs), which are evolutionarily conserved from bacteria to mammals and plants and consist of a neutral lipid core surrounded by a phospholipid monolayer (Murphy, 2012). Once thought to be simple static depots of energy-rich lipid reserves, LDs are now increasingly viewed as bona fide subcellular organelles with dedicated and perhaps dynamic sets of surface-associated proteins that are required for the biogenesis and function of LDs in various metabolic and developmental contexts and tissue/cell types (Farese and Walther, 2009; Chapman et al., 2012). For instance, perilipins, which are members of the PAT domain-containing protein family and the most abundant proteins on the surface of LDs in mammalian cells, promote the formation of nascent LDs from discrete regions of the endoplasmic reticulum (ER; Greenberg et al., 1991; Jacquier et al., 2013). Current models suggest that perilipins target in a post-translational manner to regions of the ER that are involved in LD biogenesis, where they help to stabilize the nascent LDs (Brasaemle et al., 1997; Jacquier et al., 2011, 2013). Perilipins also serve functional roles on the surface of mature, cytosolic LDs by either blocking or

[1] This work was supported by the U.S. Department of Energy, Division of Biological and Environmental Research (grant no. DE–FG02–09ER64812/DE–SC0000797 to K.D.C., J.M.D., and R.T.M.), the Natural Sciences and Engineering Research Council of Canada (grant no. 217291 to R.T.M.) and the University of Guelph (Research Chair to R.T.M.), the U.S. Department of Agriculture Agricultural Research Service (project no. 2020–21000–012–00D to J.M.D.), the Canadian Institutes of Health Research (grant no. 10490 to D.W.A.), and the National Science Foundation (grant no. 1126205 to the University of North Texas).

* Address correspondence to john.dyer@ars.usda.gov and rtmullen@uoguelph.ca.

The author responsible for distribution of materials integral to the findings presented in this article in accordance with the policy described in the Instructions for Authors (www.plantphysiol.org) is: Robert T. Mullen (rtmullen@uoguelph.ca).

S.K.G., S.P., M.P., O.Y., Y.C., and P.W. performed the experiments; D.W.A., K.D.C., J.M.D., and R.T.M. designed the experiments, and all authors interpreted and evaluated data and suggested additional experiments; J.M.D. and R.T.M. wrote the article with contributions of all the authors.

www.plantphysiol.org/cgi/doi/10.1104/pp.15.01977

recruiting lipase enzymes responsible for the metabolism of stored lipids (Lass et al., 2006; Farese and Walther, 2009; Yang et al., 2012a). In green algae, the most abundant protein associated with LDs is the MAJOR LIPID DROPLET PROTEIN, which is not only required for the formation of properly sized LDs but also influences the phospholipid composition of the LD membrane and recruits different sets of surface-associated proteins, depending on the physiological status of the cell (Moellering and Benning, 2010; Tsai et al., 2015). Thus, in some cases, the most abundant coat proteins are involved in both biogenetic and functional aspects of the organelles.

In plants, the best characterized LD-associated protein is oleosin, which is the most abundant protein on LDs in oilseeds, where LDs accumulate during seed development and then are mobilized following germination in order to provide carbon and energy for seedling growth (Huang, 1996; Siloto et al., 2006; Miquel et al., 2014; Deruyffelaere et al., 2015; Laibach et al., 2015). Oleosins are small, hydrophobic proteins that initially insert cotranslationally into the ER membrane (Beaudoin and Napier, 2002), where, analogous to perilipins, they are thought to help promote the formation of nascent LDs via budding from the ER's outer leaflet, possibly by partitioning neutral lipids within the ER bilayer (Jacquier et al., 2013) and/or aiding in stabilizing the curvature of the ER membrane (Roux et al., 2005). Oleosins also function on the surface of cytosolic LDs to prevent the fusion of LDs during seed desiccation and may serve to recruit lipases that are responsible for the metabolism of the stored TAGs during postgerminative growth (Hsieh and Huang, 2004). Oleosins, however, appear to be expressed almost exclusively in seeds and pollen grains, both of which undergo desiccation, and they are almost entirely absent in vegetative tissue/cell types (Huang, 1996; Levesque-Lemay et al., 2016). These observations raise the question of what other LD-associated protein(s) are involved in the biogenesis and regulation of LDs in all other, nonseed tissues in plants. In leaves, for instance, the proteins associated with LDs and the roles of the organelle are poorly understood. There is emerging evidence, however, that LDs participate in important ways in the stress response and plant growth and development (Shimada et al., 2014, 2015; Shimada and Hara-Nishimura, 2015); thus, it is important to identify and characterize the proteins associated with LDs in vegetative cells to begin to elucidate the mechanisms that regulate these processes.

To gain insight into the proteins involved in the biogenesis and functionality of LDs in nonseed tissues, we previously performed a proteomics analysis of LDs isolated from the mesocarp of avocado (*Persea americana*), an oil-rich, nonseed tissue that lacks oleosin proteins (Horn et al., 2013). Two of the top five most abundant proteins associated with these LDs were annotated as small rubber particle proteins (SRPPs), which was somewhat surprising, given that avocado does not contain any appreciable amounts of rubber. The SRPPs and a closely related protein called rubber elongation factor (REF) are major constituents of rubber particles, which are LD-like organelles that compartmentalize polyisoprenes, rather than TAGs, in rubber-producing plants such as *Hevea brasiliensis* (rubber tree) and *Taraxacum kok-saghyz* (Russian dandelion; Berthelot et al., 2014a, 2014b). Given that avocado lacks rubber, we termed these SRPP-like proteins lipid droplet-associated proteins (LDAPs; Gidda et al., 2013; Horn et al., 2013). The LDAPs are broadly conserved in higher to lower plant species, yet they are specific to the plant kingdom (Gidda et al., 2013; Horn et al., 2013; Divi et al., 2016). These genes are also strongly induced during stress responses in certain plant species, and ectopic overexpression of the gene in transgenic plants improved tolerance to a variety of stress conditions (Kim et al., 2010; Seo et al., 2010). As such, it appears that there may be a potential role for the LDAPs both in LD biogenesis and during plant stress responses.

To gain insight into the role(s) of LDAPs, and also to learn more about the physiological importance of LDs in vegetative tissues in general, we characterized the three LDAPs of Arabidopsis (*Arabidopsis thaliana*; LDAP1–LDAP3) using a combination of protein-targeting studies, liposome-binding assays, and alteration of expression in planta. Overall, the results revealed that all three Arabidopsis LDAPs target with high specificity to the LD surface and play important, and likely shared, roles in LD biogenesis, maintenance, and neutral lipid homeostasis in vegetative cell types. We also show that LD abundance in Arabidopsis leaves is diurnally regulated and that all three LDAPs are important for this process. Furthermore, while LDAPs were not required for proper LD biogenesis in seeds, at least one of the LDAPs, namely LDAP1, was essential for the proper compartmentalization and maintenance of LDs during postgerminative seedling growth. Finally, we demonstrate that LDs proliferate in response to different abiotic stresses, specifically cold and heat, and that specific LDAPs are involved in these responses. Taken together, these results shed light on LD biogenesis and function in vegetative tissues, identify LDAPs as key players in many of these processes, and open new avenues of research for understanding potential roles of LDs in carbon/energy balance in relation to diurnal cycling as well as lipid signaling and/or membrane remodeling during plant stress responses.

RESULTS

Arabidopsis *LDAP* Genes Are Nearly Constitutively Expressed, and the Proteins Localize to the Surface of LDs in Vegetative Cell Types

The three *LDAP* genes of Arabidopsis (*LDAP1*, *LDAP2*, and *LDAP3*) encode proteins of 235, 246, and 240 amino acids, respectively, that are moderately conserved at the polypeptide sequence level (18% identical and 47% similar; Fig. 1A). All three proteins lack any obvious

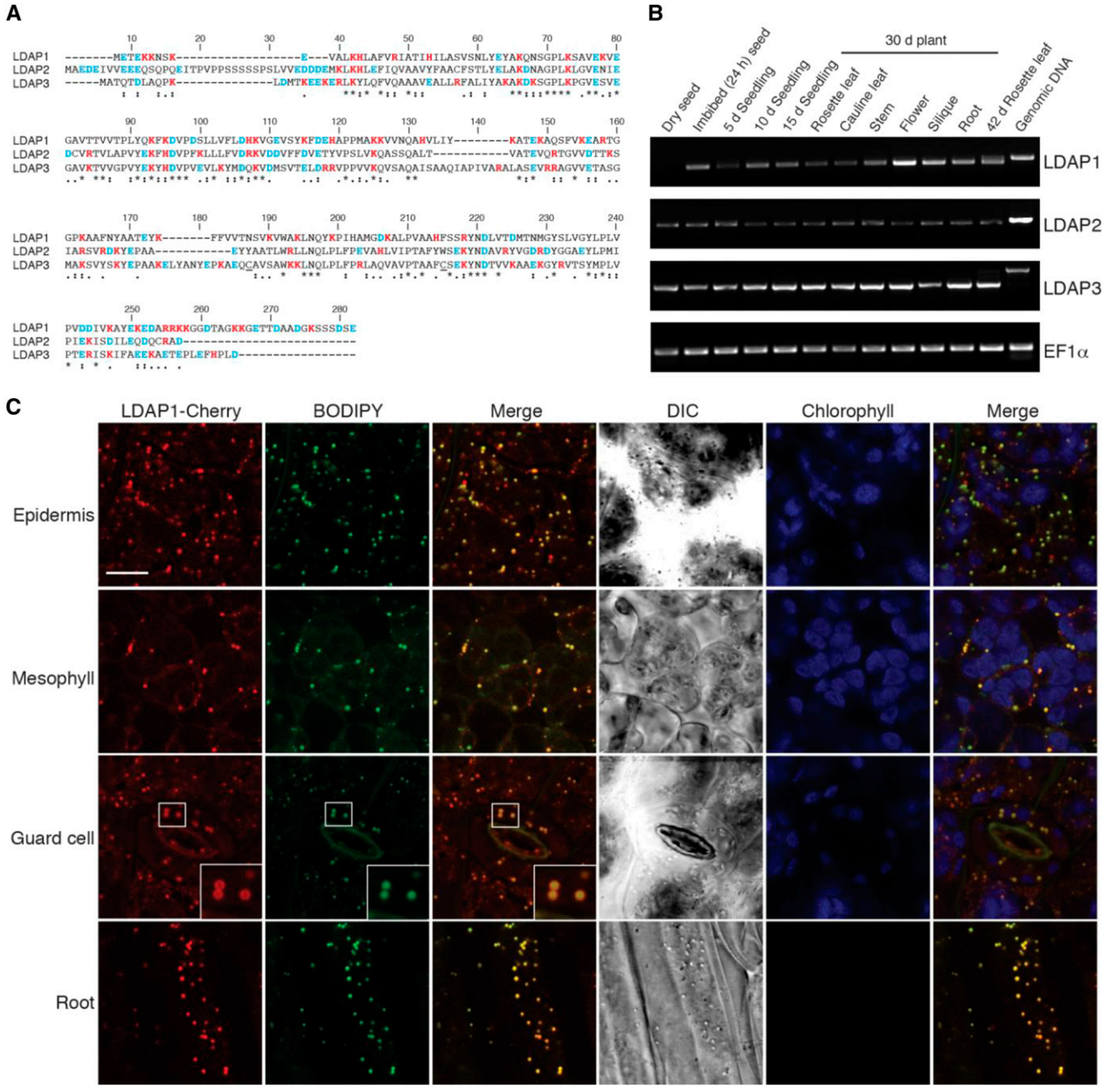

Figure 1. Properties of Arabidopsis LDAPs. A, Deduced polypeptide sequence alignment, with positively and negatively charged residues highlighted in red and blue and identical and similar residues indicated with asterisks and colons or periods, respectively. The two Cys residues in LDAP3 (positions 168 and 196) described in the LDAP3 liposome-binding assays (Fig. 2C) are underlined. B, Reverse transcription (RT)-PCR analysis of *LDAP* gene expression in various tissues and developmental stages, as indicated by labels. ELONGATION FACTOR1-α (EF1α) served as an endogenous control. Additional controls for RT-PCR primer specificity are shown in Supplemental Figure S7B. C, Representative CLSM images of LDAP1-Cherry localization in various vegetative cell types of 15-d-old stably transformed Arabidopsis seedlings. Note the colocalization of LDAP1-Cherry with BODIPY-stained LDs in each cell type, as indicated by labels. Boxes represent the portion of the cell shown at higher magnification, revealing an LDAP1-Cherry torus-shaped fluorescence pattern surrounding the BODIPY-stained TAG core and indicating that LDAP1 is localized to the surface of LDs. Similar subcellular localizations for LDAP2 and LDAP3 in Arabidopsis are shown in Supplemental Figure S2. Also shown for each cell type are the corresponding chlorophyll autofluorescence and differential interference contrast (DIC) images. Bar = 20 μm.

subcellular targeting signals and do not contain any predicted hydrophobic membrane-spanning domains, unlike oleosin, which has an extensive hydrophobic region that penetrates into the LD core (van Rooijen and Moloney, 1995; Abell et al., 1997, 2004; Supplemental Fig. S1). In fact, each of the LDAPs is conspicuously

hydrophilic in character, with a preponderance of positively and negatively charged residues that are distributed throughout the length of the protein sequence (Fig. 1A). Analysis of gene expression revealed that all three *LDAPs* are constitutively expressed in a variety of plant tissues/organs and developmental stages, although *LDAP3* expression appears to be higher than *LDAP1* and *LDAP2* expression overall and *LDAP1* expression is relatively lower in dry seeds and induced in imbibed seeds (Fig. 1B).

Prior studies revealed that LDAP3, which is the Arabidopsis protein with the highest sequence similarity compared with the avocado LDAPs, localized to LDs when expressed transiently in tobacco (*Nicotiana tabacum*) 'Bright Yellow-2' (BY-2) suspension-cultured cells (Horn et al., 2013). To further characterize the subcellular localization of the LDAPs, but in the native plant system, we generated stable transgenic lines of Arabidopsis expressing single-gene copies of Cherry fluorescent protein-tagged LDAP1, LDAP2, or LDAP3 and then evaluated each fusion protein relative to BODIPY-stained LDs using confocal laser-scanning microscopy (CLSM). As shown in Figure 1C and Supplemental Figure S2, each LDAP localized specifically to LDs in epidermal cells, mesophyll, guard cells, and root cells. High-magnification images of the LDs in guard cells further revealed that the LDAPs encircled the BODIPY-stained TAG core, indicating that the LDAPs were localized to the surface of LDs. Moreover, comparisons with chlorophyll autofluorescence revealed that the localization of all three LDAPs was distinct from chloroplasts, confirming that they were localized to cytosolic LDs and not plastoglobuli (Fig. 1C; Supplemental Fig. S2).

The Targeting of LDAP3 to LDs Requires Nearly the Entire Protein Sequence and Involves Detergent-Sensitive Interactions, But Targeting Fidelity Is Not Determined by Phospholipid Composition Alone

The lack of any obvious hydrophobic regions in the LDAP polypeptide sequences (Fig. 1A; Supplemental Fig. S1), coupled with their exclusive localization to LDs in vivo (Fig. 1C; Supplemental Fig. S2), raises the intriguing question of how these proteins target with such high specificity to the LD surface. To gain insight into this process, we used LDAP3 as a model LDAP to investigate cis-acting targeting signals, interactions with the LD surface in vivo, and the ability to bind to synthetic liposomes in vitro.

As shown in Figure 2A (top row, left three images), transient expression of LDAP3 appended to the GFP in tobacco cv BY-2 suspension cells, which serve as a well-established model cell system for intracellular protein targeting studies (Brandizzi et al., 2003; Lingard et al., 2008), resulted in localization of the fusion protein to the cytosol and LDs. Notably, when linoleic acid (LA) was included in the culture medium, there was a significant proliferation of LDs in the cells (Supplemental Fig. S3), and a greater proportion of the LDAP3-GFP was located on LDs rather than the cytosol (Fig. 2A), suggesting that LDAP3 targets to LDs from the cytosol based on the presence of the organelle. Similar localization patterns were observed for LDAP1 and LDAP2 expressed in cv BY-2 cells that either were or were not incubated with LA (Supplemental Fig. S4A). As also shown in Figure 2A, any truncation of the LDAP3 protein by the removal of amino acid sequences from either the C or N terminus, or an internal region of the protein, disrupted its localization to LDs in cv BY-2 cells incubated with LA. Instead, all of the various mutant proteins mislocalized to the cytosol (Fig. 2A), suggesting that the entire LDAP sequence is required for proper LD targeting. Furthermore, the type and/or position of the fluorescent protein moiety appended to LDAP3 did not influence targeting to LDs (Supplemental Fig. S4B) or, in the case of the mutant protein LDAP3ΔC46, its mistargeting to cytosol (Supplemental Fig. S4C).

To begin to characterize the biophysical interactions between LDAPs and the surface of LDs, we again employed the cv BY-2 cell system along with differential detergent permeabilization and lipid extraction experiments, which are often used to probe the relationships between proteins and membranes in vivo (Wolvetang et al., 1990; Lee et al., 1997). LDAP3-GFP was transiently expressed in cv BY-2 cells incubated with LA to allow for its association with LDs, as above. Cells were then permeabilized with either digitonin, which disrupts primarily the plasma membrane, due to interaction with the sterols that are enriched in this membrane bilayer, or Triton X-100, which more extensively and nonselectively interacts with all cellular membranes (Wolvetang et al., 1990; Lee et al., 1997, Jamur and Oliver, 2010). As shown in Figure 2B, the association of LDAP3-GFP with LDs was not disrupted by digitonin but was disrupted when cells were treated with Triton X-100 (i.e. LDAP3 localized predominantly to the cytosol when cells were incubated with Triton X-100). Notably, BODIPY-stained LDs were still present in both sets of cells treated with either digitonin or Triton X-100, indicating that at least the lipid core of the LDs remained intact in both conditions. As controls, parallel experiments were conducted using GFP-tagged versions of DIACYLGLYCEROL ACYLTRANSFERASE2 (DGAT2), an integral ER membrane protein (Shockey et al., 2006), and OLEOSIN ISOFORM1 (OLEO1), which, as mentioned previously, possesses a hydrophobic domain that anchors deeply within the LD core (van Rooijen and Moloney, 1995; Abell et al., 1997, 2004). Neither GFP-DGAT2 in the ER nor OLEO1-GFP at LDs was extracted by digitonin or Triton X-100 (Fig. 2B), indicating that LDAP3 interacts with the LD surface in a detergent-sensitive fashion that is distinct from the mechanism employed by oleosin.

We next tested whether LDAP3 can bind directly to a phospholipid surface using a Förster resonance energy transfer (FRET)-based assay and biomimetic liposome membranes (Lovell et al., 2008). LDAP3 contains two endogenous Cys residues at positions

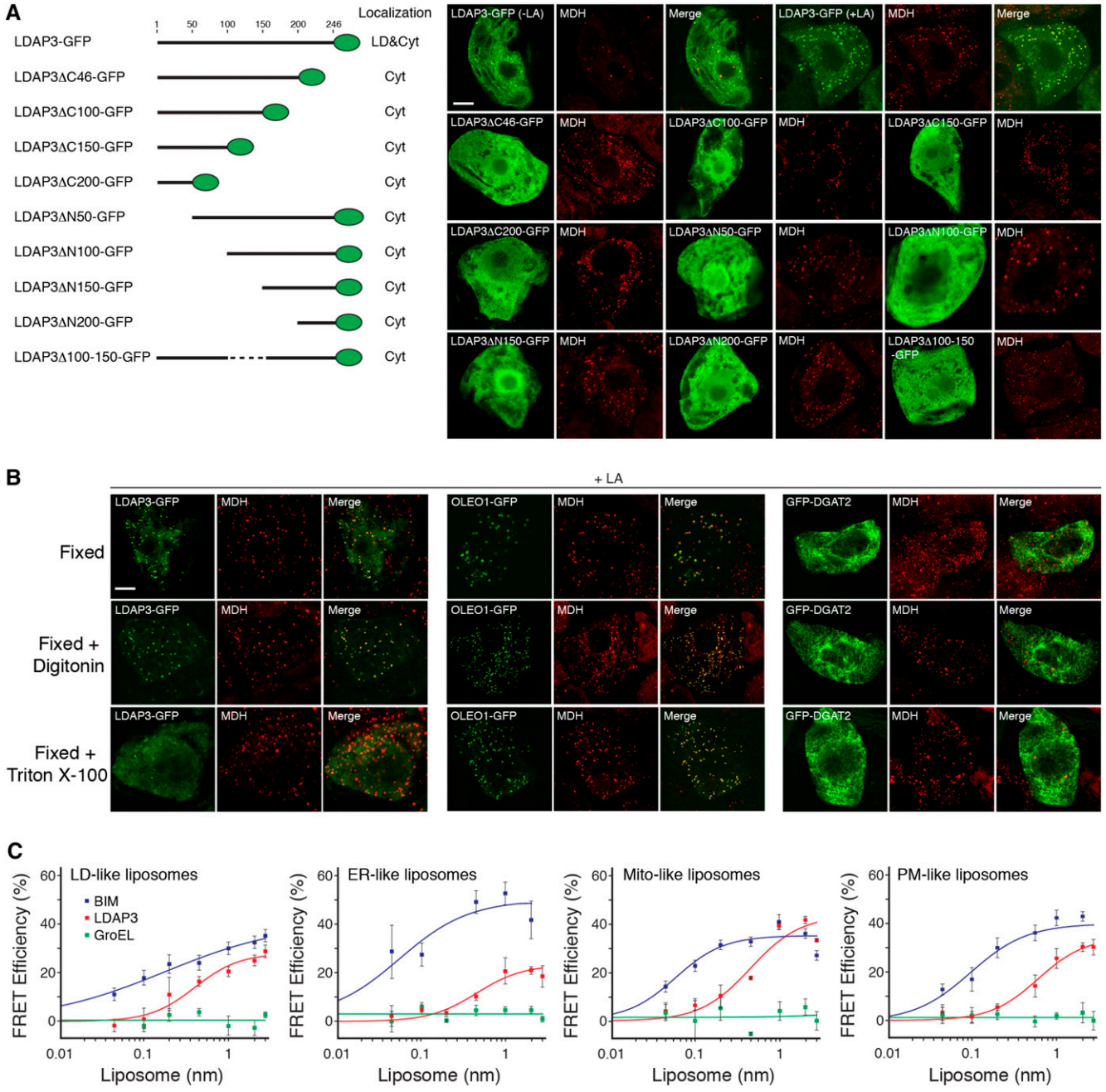

Figure 2. Subcellular targeting and biophysical interactions of LDAP3 with LDs and synthetic liposomes. A, Truncation analysis of LDAP3 in tobacco cv BY-2 cells. The cv BY-2 cells were transiently transformed with full-length or a modified version of LDAP3-GFP, stained with the neutral lipid dye monodansylpentane (MDH), and imaged using CLSM. The cv BY-2 cells were incubated with LA to induce LD proliferation (Supplemental Fig. S3), unless indicated otherwise. Shown on the left are cartoon representations of the various LDAP3-GFP constructs and their corresponding subcellular localization(s) in cv BY-2 cells (Cyt, cytosol). Shown on the right are representative micrographs for each LDAP3-GFP protein along with the corresponding MDH-stained LDs (false-colored red) in the same cell. Bar = 10 μm. B, Biophysical analysis of LDAP3 interaction with LDs in vivo. LDAP3-GFP, OLEO1-GFP, or GFP-DGAT2 was expressed transiently (as indicated by labels) in cv BY-2 cells incubated with LA. Cells were then fixed and extracted with either digitonin, which perturbs primarily the plasma membrane, or Triton X-100, which perturbs all cellular membranes, and then stained with MDH. Note that LDAP3 was resistant to digitonin extraction, but, unlike OLEO1 and DGAT2, LDAP3 was sensitive to Triton X-100 extraction, whereby the majority of protein was dissociated to the cytosol (left images). Bar = 10 μm. C, LDAP3 synthetic liposome-binding assays. Recombinant LDAP3 was purified (Supplemental Fig. S5), labeled at its single Cys with donor fluorophore, then mixed with a range of concentrations of acceptor fluorophore-labeled liposomes of various phospholipid compositions (Supplemental Table S1). Binding was assessed based on FRET efficiency (i.e. based on the change in fluorescence of the fluor-labeled donor protein when acceptor fluor-containing liposomes were present).

Table I. *Interaction of LDAP3 with liposomes of various phospholipid compositions*

For specific phospholipid compositions of synthetic liposomes, see Supplemental Table S1. BIM, Bcl-2-interacting mediator of cell death; GroEL, chaperonin 60 heat shock protein.

Liposome	K_d[a]		
	LDAP3	BIM	GroEL
LD-like liposomes	0.33 ± 0.08	ND[b]	ND
ER-like liposomes	0.38 ± 0.11	0.045 ± 0.025	ND
Mitochondrial outer membrane-like liposomes	0.35 ± 0.11	0.048 ± 0.013	ND
Plasma membrane-like liposomes	0.48 ± 0.11	0.079 ± 0.08	ND

[a]Calculated dissociation constant values for protein-liposome-binding assays presented in Figure 2B. Data presented are averages ± SE from three separate experiments. [b]ND, Not determined. This represents samples where a binding curve that saturates was not observed (see Fig. 2B); therefore, it was not possible to calculate an accurate dissociation constant value.

168 and 196 (Fig. 1A); hence, mutation of Cys-196 to Ala resulted in a single Cys variant [i.e. LDAP3 ($C^{196}A$)] that could be specifically labeled with a fluorescent dye. Recombinant, His-tagged LDAP3 was expressed in bacteria and then purified using nickel-affinity chromatography (Supplemental Fig. S5A), followed by cobalt-affinity chromatography (Supplemental Fig. S5B), and then labeled with the donor fluorophore Alexa-568. The labeled LDAP3 protein was then incubated with a range of concentrations of synthetic liposomes of various phospholipid compositions labeled with the long-chain dialkylcarbocyanine dye (DiD) serving as the acceptor fluorophore (Supplemental Table S1). The FRET efficiency was measured using fluorescence spectroscopy, and where binding saturated, dissociation constants were calculated. As shown in Figure 2C and Table I, LDAP3 bound to liposomes composed of phospholipids resembling the LD surface, whereas the protein BIM, which is known to bind to mitochondrial liposomes (Lovell et al., 2008), interacted with LD liposomes only poorly and binding did not saturate over the concentration range tested. While these data might suggest that LDAP3 shows preferential association with the LD surface, LDAP3 also bound with similar affinity to liposomes composed of phospholipids typical of the ER, outer mitochondrial, or plasma membranes (Fig. 2C; Table I). In contrast, BIM bound to these liposomes with almost 1 order of magnitude higher affinity than LDAP3, whereas the negative control protein, the bacterial chaperonin protein GroEL, did not bind to any of the liposomes tested, as expected. Taken together, these data suggest that, while LDAP3 can bind to phospholipid membranes, it does so with relatively low overall affinity that does not distinguish between different phospholipid compositions. As such, protein-lipid interactions alone are not likely to account for the high level of organellar targeting specificity observed for LDAPs in vivo.

LDAPs Are Involved in the Dynamic Modulation of LD Abundance during the Diurnal Cycle in Arabidopsis Leaves

To begin to gain insight to the function(s) of LDAPs in vivo, we characterized LD dynamics in Arabidopsis lines that were either disrupted for *LDAP* gene expression or stably overexpressed Cherry-tagged versions of each protein. LDs in all lines were visualized in leaves using BODIPY staining and CLSM. In preliminary experiments, we noted that LD abundance in leaves varied considerably during the diurnal cycle. Indeed, quantitative analysis of LDs in leaves of 15-d-old wild-type seedlings over a typical day/night growth cycle (i.e. 16 h of light/8 h of dark) revealed that the highest numbers of LDs were observed at the end of the night, while the lowest numbers were seen at the end of the day (Fig. 3A). Although these differences in LD abundance in leaves did not fully correlate with *LDAP* expression, perhaps with the exception of *LDAP3* (Supplemental Fig. S6A), they do suggest that LD abundance in leaves is regulated in part by physiological differences associated with light and dark metabolism. In support of this premise, incubation of plants in extended dark or light resulted in a persistent high or low abundance of LDs, respectively (Supplemental Fig. S6).

To determine whether LDAPs are important for the modulation of LD abundance during diurnal cycling, the number of LDs was assessed in leaves of seedlings at the end of the day for *LDAP*-overexpressing lines, when LDs are least abundant in the wild type, and at the end of the night for the *LDAP*-disrupted lines, when LDs are most abundant in the wild type. As shown in Figure 3B,

Figure 2. (*Continued.*)
While LDAP3 (red curves) exhibited different maximal FRET efficiencies at saturation for liposomes composed of different lipids, the protein displayed similar moderate binding to all liposomes in a manner that was stronger than the negative control protein (GroEL; green curves) but weaker than the positive control protein (BIM; blue curves). The highest concentration of liposomes is the largest amount that could be added to the reactions. Calculated dissociation constant values for protein-liposome-binding assays are presented in Table I. Mito, Mitochondria; PM, plasma membrane.

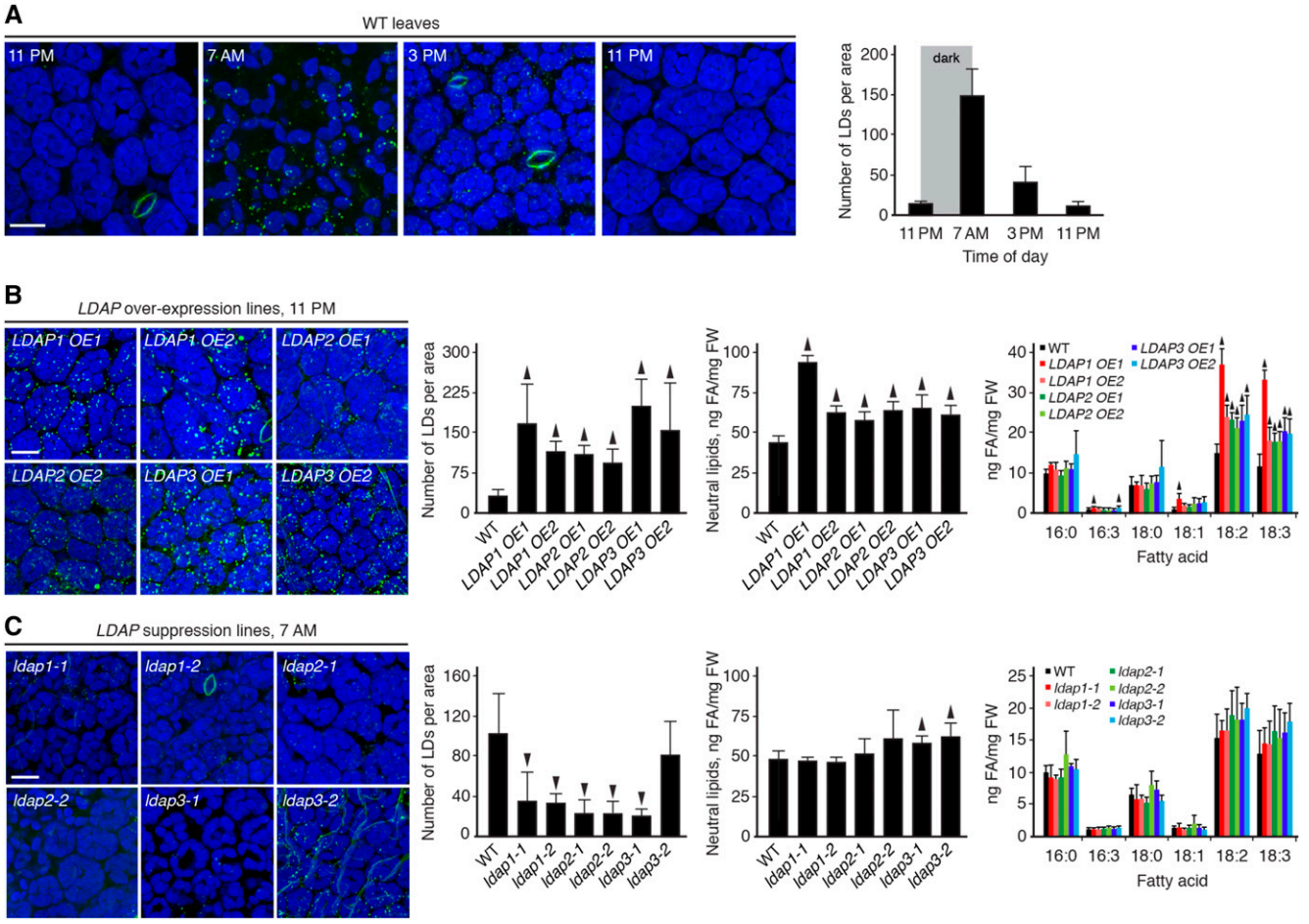

Figure 3. LD abundance in Arabidopsis leaves during the diurnal cycle and in *LDAP* transgenic plants. A, Diurnal regulation of LD abundance in Arabidopsis leaves. Wild-type (WT) plants were grown on one-half-strength Murashige and Skoog (MS) plates for 15 d in a 16-h/8-h day/night cycle (lights on at 7 AM and off at 11 PM), then leaves were harvested at the indicated times and LDs were examined by BODIPY staining and CLSM. Representative images are shown on the left, and quantifications of LDs are shown on the right. B, Overexpression of *LDAPs* in leaves. Two independent, homozygous, single-copy lines were generated for overexpression of each *LDAP* (i.e. LDAP-Cherry; Supplemental Fig. S7), then leaves were collected and imaged at 11 PM, when LD abundance is low in the wild type (see A). Representative CLSM images of each plant line are shown on the left, and quantifications of LDs are shown in the bar graph on the right. The graphs in the middle show neutral lipid content and composition of plant leaves showing increases in total neutral lipids due primarily to increases in polyunsaturated (i.e. 18:2 and 18:3) fatty acids (FA). C, Suppression of *LDAPs* in leaves. Two independent T-DNA and/or RNAi lines were generated for each LDAP (Supplemental Fig. S7), then leaves were collected and imaged (using CLSM) at 7 AM, when LD abundance is high in the wild type (see A). All of the LDAP-disrupted lines, except *ldap3-2*, showed decreases in LD abundance (left graph) and no or moderate changes in neutral lipid content (middle graph) or fatty acid composition (right graph). Values of quantified LDs in A to C represent averages and SD from three biological replicates. Values of lipids in B and C represent averages and SD from five biological replicates. Arrowheads represent statistically significant differences above (pointing up) or below (pointing down) the wild-type value as determined by Student's *t* test ($P < 0.05$). FW, Fresh weight. Bars in A, B, and C = 20 μm.

the overexpression of any one of the three *LDAP* genes, with two independent events for each transgene (for genotyping and relative gene expression in transgenic lines, see Supplemental Fig. S7), resulted in a significant increase in LD abundance at the end of the day in comparison with the wild type. Conversely, disruption of *LDAP* expression through either transfer DNA (T-DNA) knockout or RNA interference (RNAi) in two independent events (Supplemental Fig. S7) significantly decreased LD abundance at the end of the night in comparison with the wild type (Fig. 3C). Collectively, these data reveal that the LDAPs are important for the proper modulation of LD abundance during the diurnal cycle.

To determine whether the observed differences in LD abundance caused by overexpression or disruption of LDAPs resulted in any changes in neutral lipid levels, total lipids were extracted from leaves of 15-d-old seedlings, then neutral lipids were isolated by solid-phase extraction and analyzed by gas chromatography and flame ionization detection. As shown in Figure 3B and

Supplemental Figure S8, all lines overexpressing the *LDAP* genes showed significant increases in total neutral lipid content, and analysis of fatty acid composition showed an enrichment in 18:2 and 18:3 fatty acids. In *LDAP*-disrupted plant lines, however, there were no significant decreases in neutral lipid content, although *ldap3-1* and *ldap3-2* mutant lines did show modest increases in neutral lipid abundance (Fig. 3C; Supplemental Fig. S8).

LDs Proliferate during Abiotic Stress Responses in Arabidopsis Leaves, and LDAP3 and LDAP1 Are Required for Normal LD Proliferation during Cold and Heat Stress, Respectively

Prior studies revealed that *LDAP* genes are strongly induced during abiotic stress responses in a variety of plant species (Sookmark et al., 2002; Priya et al., 2007; Kim et al., 2010; Seo et al., 2010; Fricke et al., 2013), and more recent studies have shown that neutral lipid content, particularly TAG, is increased in response to cold or heat (Mueller et al., 2015; Tarazona et al., 2015). Given that LDAPs target to LDs (Figs. 1 and 2; Supplemental Fig. S2) and can modulate both LD and neutral lipid abundance (Fig. 3), we hypothesized that abiotic stress responses would induce a proliferation of LDs in plant leaves. Digital northern data available at the eFP Browser (Winter et al., 2007) indicated that, of the two Arabidopsis *LDAP* genes represented on the ATH1 whole-genome chip, namely *LDAP1* and *LDAP3*, both are up-regulated during cold stress response, and *LDAP1*, in particular, is strongly up-regulated during heat stress response (Winter et al., 2007).

To determine whether LD proliferation is part of the cold stress response of Arabidopsis, 15-d-old wild-type seedlings were cultivated under control or cold temperature conditions (4°C) for 24 h, and then LD abundance was determined using BODIPY staining and CLSM. As shown in Figure 4A, wild-type leaves showed an approximately 10-fold increase in the number of LDs in response to cold temperature, and RT-PCR analysis confirmed that both *LDAP1* and *LDAP3* were induced by this treatment. *LDAP2*, on the other hand, was not as strongly or consistently induced. Notably, a similar induction of LD proliferation was observed in *ldap1-1* or *ldap2-1* mutants, but *ldap3-1* plants showed a significant reduction in LD abundance during cold temperature response (Fig. 4A), suggesting that LDAP3 participates in some unique way in the proliferation of LDs during cold stress treatment.

As shown in Figure 4B, incubation of 15-d-old wild-type Arabidopsis seedlings at high temperature (37°C) for 1 h also promoted a significant increase in LD abundance in comparison with control plants, and RT-PCR analysis revealed that *LDAP1* expression, consistent with the above-mentioned e-northern data (Winter et al., 2007), was more strongly induced in comparison with the other two *LDAPs*. Analysis of LD proliferation in the *ldap* mutants further revealed a similar proliferation of LDs in the *ldap2-1* and *ldap3-1* mutants compared with the wild type, but the proliferation in the *ldap1-1* mutant was reduced significantly (Fig. 4B). Collectively, these data suggest that, similar to the role of LDAP3 in cold stress adaptation, LDAP1 somehow participates in a unique way during the proliferation of LDs during heat stress.

LDAP1 Is Specifically Required for Proper Neutral Lipid Compartmentation and Breakdown during the Transition from Seed Dormancy to Postgerminative Growth

The seeds of many plants, including Arabidopsis, synthesize large amounts of TAG that are stored in oleosin-coated LDs in mature seeds. Upon imbibition and seed germination, the oleosin proteins are rapidly degraded and TAG is mobilized to provide carbon and energy in support of postgerminative growth (Hsieh and Huang, 2004; Deruyffelaere et al., 2015). To elucidate the potential roles of LDAPs in seed biology, we first examined the effects of overexpressing LDAPs on LD morphology and oil accumulation in mature, dry seeds. CLSM analysis of mature embryos from wild-type and *LDAP*-overexpressing plant lines showed no obvious differences in number or morphology of LDs (Fig. 5A), and total oil content and fatty acid composition of dry seeds were similar to the wild type, although some lines did show modest but statistically significant changes (Fig. 5, C and D). Furthermore, analysis of the LDAP-Cherry fluorescence patterns in dry seeds revealed that the proteins were located primarily in distinct, punctate, and/or aggregated structures that did not colocalize with BODIPY-stained LDs (Fig. 5A). One day after the initiation of seed germination, however, LDAP-Cherry localization was conspicuously altered, with at least a portion of the fluorescence pattern attributable to each protein encircling some of the BODIPY-stained LDs (Fig. 5B). Taken together, these data suggest that LDAPs do not play a prominent role in LD biogenesis and TAG accumulation during seed development but do associate with LDs during postgerminative growth.

Suppression of *LDAP* gene expression also had no apparent effects on LD number or morphology in mature, dry seeds (Fig. 6, A and B), but in some lines, there were moderate changes in seed oil content and fatty acid composition in comparison with the wild type (Fig. 6, C and D). At 1 d after initiation of germination, however, the LDs in the *ldap1-1* line were substantially larger in comparison with wild-type, *ldap2-1*, and *ldap3-1* lines (Fig. 6A). A similar, albeit not as pronounced, LD phenotype was observed in the *ldap1-2* mutant (Fig. 6B). Analysis of LD morphology in wild-type, *ldap1-1*, and *ldap1-2* lines using transmission electron microscopy further revealed that the images obtained via CLSM were large LDs and not aggregates of small LDs (Supplemental Fig. S9).

To determine whether the aberrant LD phenotype observed in *ldap1* mutants corresponded with any biochemical changes in neutral lipid metabolism, we quantified the degradation of TAGs during postgerminative growth. As shown in Figure 6E, total fatty

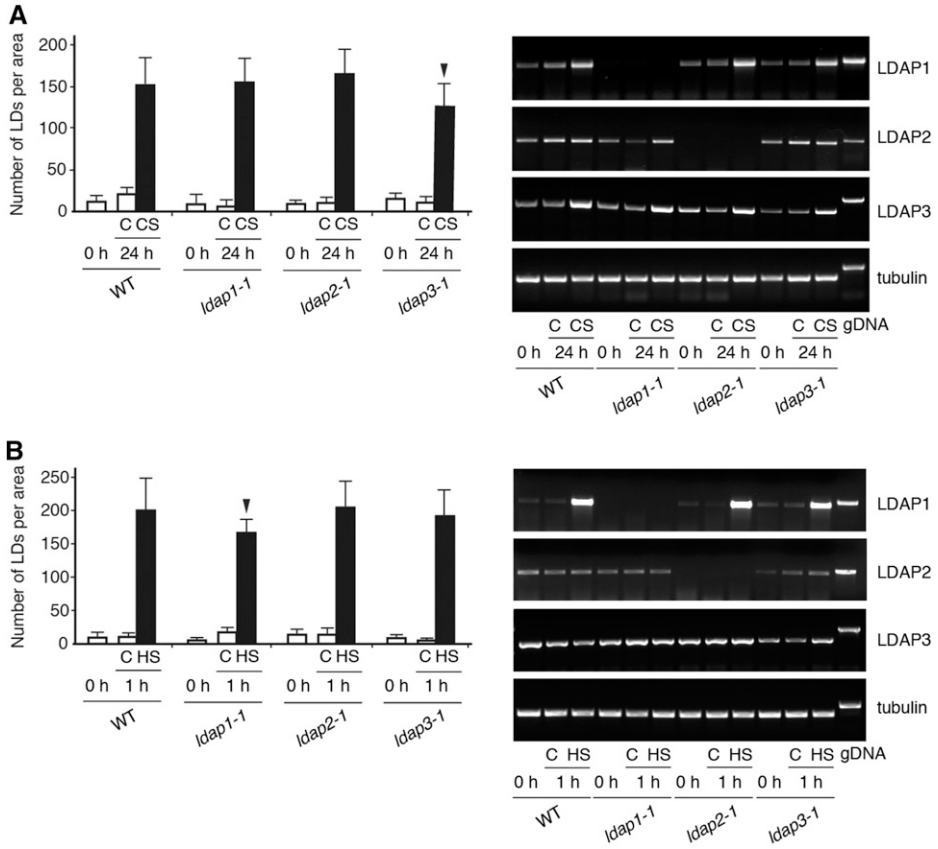

Figure 4. Proliferation of LDs and *LDAP* expression in plant leaves during abiotic stress responses. Wild-type (WT) and selected *ldap* mutant lines were grown on one-half-strength MS plates for 15 d, then a portion of the plates were transferred to either a 4°C chamber for 24 h (A) or a 37°C chamber for 1 h (B). Leaves were collected at 0 and 24 h from control (C) and cold-stressed (CS) plants or at 0 and 1 h for control or heat-stressed (HS) plants, LDs were analyzed by BODIPY staining and CLSM, and transcript levels, including tubulin serving as an endogenous control, were evaluated using RT-PCR. Wild-type plants showed an approximately 10-fold increase in LD abundance in response to cold temperature (bar graph) and significant increases in transcript levels of both *LDAP1* and *LDAP3* genes (DNA gels). Similar results were observed in the *ldap1-1* and *ldap2-1* mutants, but the abundance of LDs in *ldap3-1* during the cold temperature response was reduced significantly (bar graph). Results from heat stress experiments revealed that LDs proliferated approximately 10-fold in the wild type (bar graph), and *LDAP1* transcripts were selectively and strongly induced (DNA gels). LDs were induced similarly in *ldap2-1* and *ldap3-1* mutants but were reduced significantly in *ldap1-1* during the stress response. Values of quantified LDs represent averages and SD from three biological replicates. Arrowheads represent statistically significant differences in comparison with the wild type as determined by Student's *t* test ($P < 0.05$).

acids were significantly higher in both the *ldap1-1* and *ldap1-2* mutants at 1 d after the initiation of germination in comparison with the wild type, then the amounts became more similar to the wild type at days 2 and 4. Characterization of fatty acid composition on each day revealed that nearly all fatty acids were elevated in the *ldap1-1* and *ldap1-2* lines at 1 d after the initiation of germination, suggesting a generalized defect in seed storage oil degradation at this stage of development (Fig. 6F). By contrast, fatty acid composition at 2 and 4 d after the initiation of germination was similar to the wild type (data not shown). The similarity of total fatty acid content of the wild type and *ldap1-1* and *ldap1-2* mutants by days 2 and 4 (Fig. 6E) suggested a recovery of normal TAG packaging and metabolism at these time points. In agreement with this premise, LD morphologies of both mutant lines were more similar to the wild type at day 2 than at day 1 (Fig. 6G, compare with Fig. 6, A and B) and then indistinguishable from the wild type at day 4 (Fig. 6H). Taken together, these data point to a cellular and physiological role for LDAP1 in the proper compartmentation and mobilization of TAG during early stages of postgerminative growth.

The Transition from Seed Dormancy to Postgerminative Growth May Involve the Sequential Exchange of Oleosin and LDAP Proteins on LDs

Given that the association of LDAPs with LDs occurs 1 d after germination (Fig. 5B) and that most embryonic cell types at this stage of development have not undergone division (Bewley, 1997), it is likely that LDAPs and oleosins coexist in the same cells. To begin to examine the potential functional and perhaps biophysical

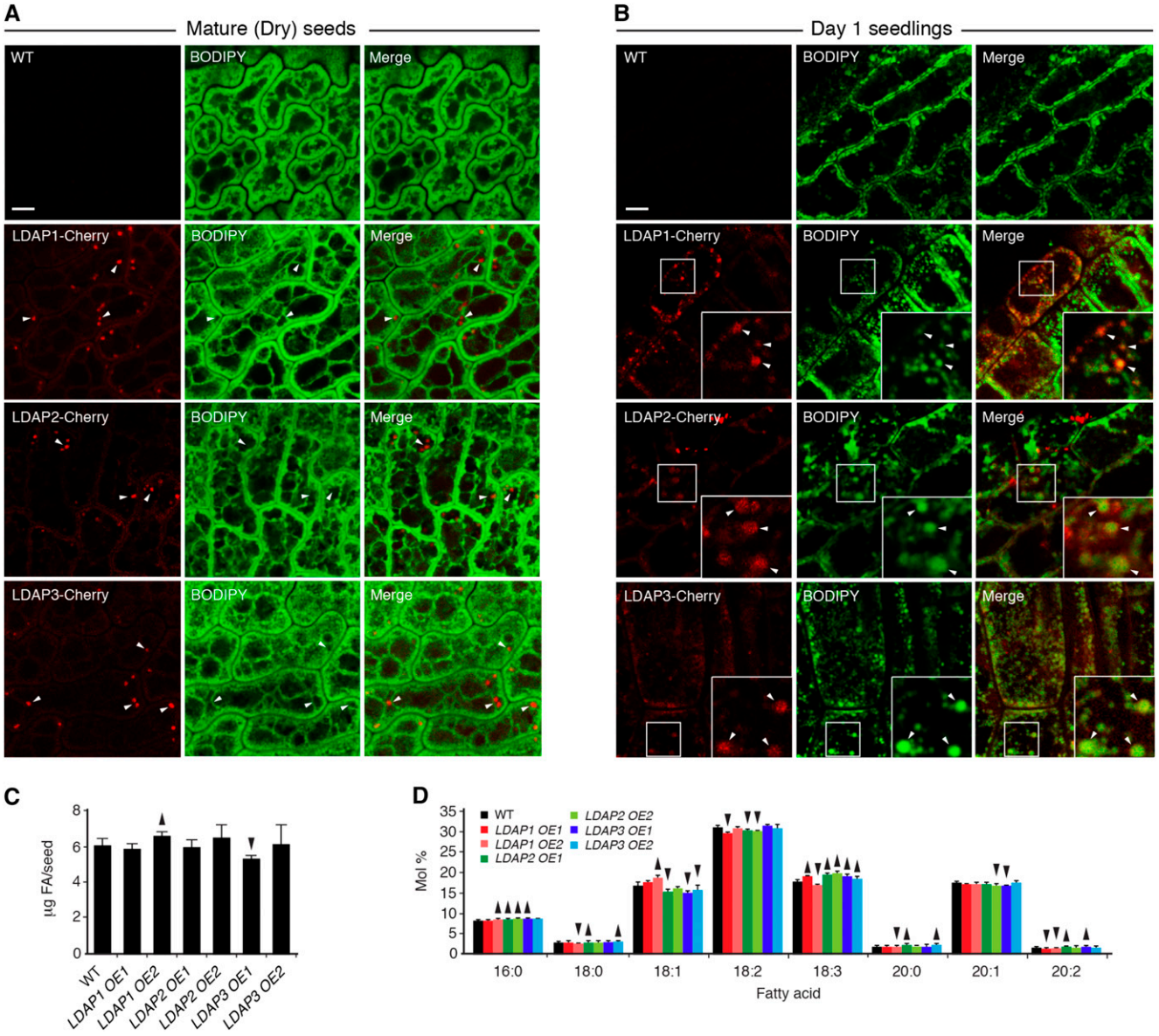

Figure 5. Effects of *LDAP* overexpression on seed development and during postgerminative growth. Two independent, single-copy, homozygous transgenic lines expressing LDAP-Cherry proteins were generated (Supplemental Fig. S7), seeds/seedlings were visualized by CLSM to evaluate LDAP localization in comparison with BODIPY-stained LDs, and seed oil content and composition were determined. A, Representative CLSM images of mature, dry seeds showing the localization of LDAPs to distinct punctate structures (left images) that do not colocalize with BODIPY-stained LDs (middle images) in merged images (right images). B, Representative CLSM images of seedlings 1 d after the onset of germination, showing the partial colocalization of LDAPs and BODIPY-stained LDs; boxes represent the portions of cells shown at higher magnification, showing the LDAP localization to torus-shaped structures surrounding BODIPY-stained TAG cores. Bars in A and B = 5 μm. C, Total fatty acids (FA) in mature seeds, showing statistically significant changes in two *LDAP* transgenic lines but no obvious trends due to *LDAP* overexpression. D, Fatty acid composition analysis of mature seeds, showing small but statistically significant changes but without any obvious trends due to *LDAP* overexpression. Values in C and D represent averages and SD of five biological replicates. Arrowheads represent statistically significant values above (pointing up) or below (pointing down) wild-type (WT) values as determined by Student's *t* test ($P < 0.05$).

relationships between oleosin and LDAPs, we took advantage of a *LEAFY COTYLEDON2* (*LEC2*)-based expression system known to induce oil production in plant leaves. LEC2 is a major seed-specific transcription factor that up-regulates many of the genes involved in oil biosynthesis, and ectopic expression of LEC2 in leaves elevates TAG production (Santos Mendoza et al., 2005; Andrianov et al., 2010; Petrie et al., 2010; Kim et al., 2013). The absolute amounts of oleosin transcripts induced in this system, however, are not as high as those observed in developing seeds (Feeney et al., 2013; Kim et al., 2013), and, as such, the level of TAG

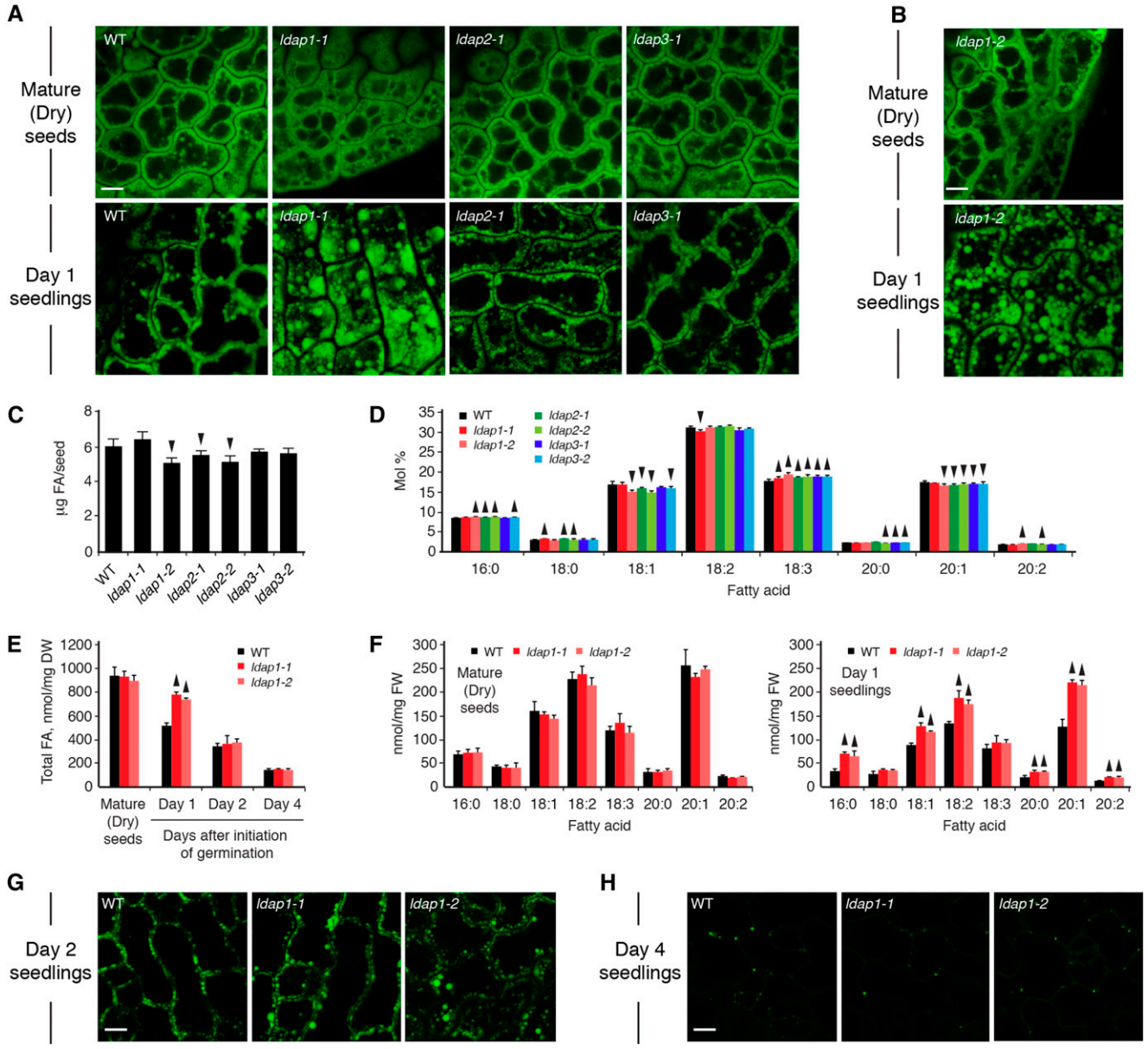

Figure 6. Effects of *LDAP* suppression on seed development and postgerminative growth. Two different homozygous suppression mutants, T-DNA knockout and/or RNAi, were generated for each *LDAP* (Supplemental Fig. S7). A, Representative CLSM images of mature, dry seeds or seedlings 1 d after the onset of germination showing LDs stained with BODIPY. Note the similarity in LD morphology in all dry seeds (top row) and the altered LD phenotype in 1-d-old *ldap1-1* seedlings in comparison with the wild type (WT), *ldap2-1*, or *ldap3-1* (bottom row). B, Dry and 1-d-old seedlings from *ldap1-2*, showing a similar phenotype in comparison with *ldap1-1* (see A). C and D, Total fatty acids (FA; C) and fatty acid compositional analysis (D) of mature seeds from the indicated plant lines, showing moderate changes in seed oil content and composition in some of the *ldap* mutants. E and F, Analysis of seed oil breakdown in wild-type, *ldap1-1*, and *ldap1-2* lines, showing total fatty acids (E) and individual fatty acid (F) amounts in mature seeds and during postgerminative growth (i.e. 1, 2, and 4 d after the initiation of germination). DW, Dry weight; FW, fresh weight. All bar graphs represent averages and SD of five biological replicates, and arrowheads represent statistically significant values above (pointing up) or below (pointing down) wild-type levels as determined by Student's *t* test ($P < 0.05$). G and H, Representative CLSM images of wild-type, *ldap1-1*, and *ldap1-2* lines at 2 d (G) and 4 d (H) after the initiation of germination, showing more similar LD morphology in comparison with the wild type in the two *ldap1* mutant lines on day 2 relative to day 1 (compare G with A and B) and normal LD morphology in both mutant lines at day 4 (compare with the wild type in H). Bars in A, B, G, and H = 5 μm.

packaging proteins is likely to be reduced relative to TAG synthesis. Evidence in support of this premise is provided in Figure 7A, which shows that transient expression of Arabidopsis LEC2 in tobacco leaves resulted in the formation of several aberrant, supersized LDs in comparison with the wild type. Coexpression

of oleosin (i.e. OLEO1-Cherry) and LEC2 in plant leaves, however, resulted in the disappearance of the supersized LDs and, instead, yielded many more regular-sized LDs (Fig. 7A), similar to when oleosin was expressed on its own. Notably, *LEC2* transcripts were confirmed to be present in cells expressing oleosin (Fig. 7B), indicating that the disappearance of the supersized LDs was not due to reduced LEC2 expression.

Similar results were observed when *LEC2* was coexpressed with any of the LDAPs (Fig. 7, A and B). Moreover, coexpression of *LEC2* with a truncated form of LDAP3 (i.e. LDAP3ΔC46-Cherry) that was shown previously to mistarget to the cytosol (Supplemental Fig. S4C) did not reduce the presence of the supersized LDs (Fig. 7A), indicating that association of LDAP with the LD surface was required for proper LD compartmentation.

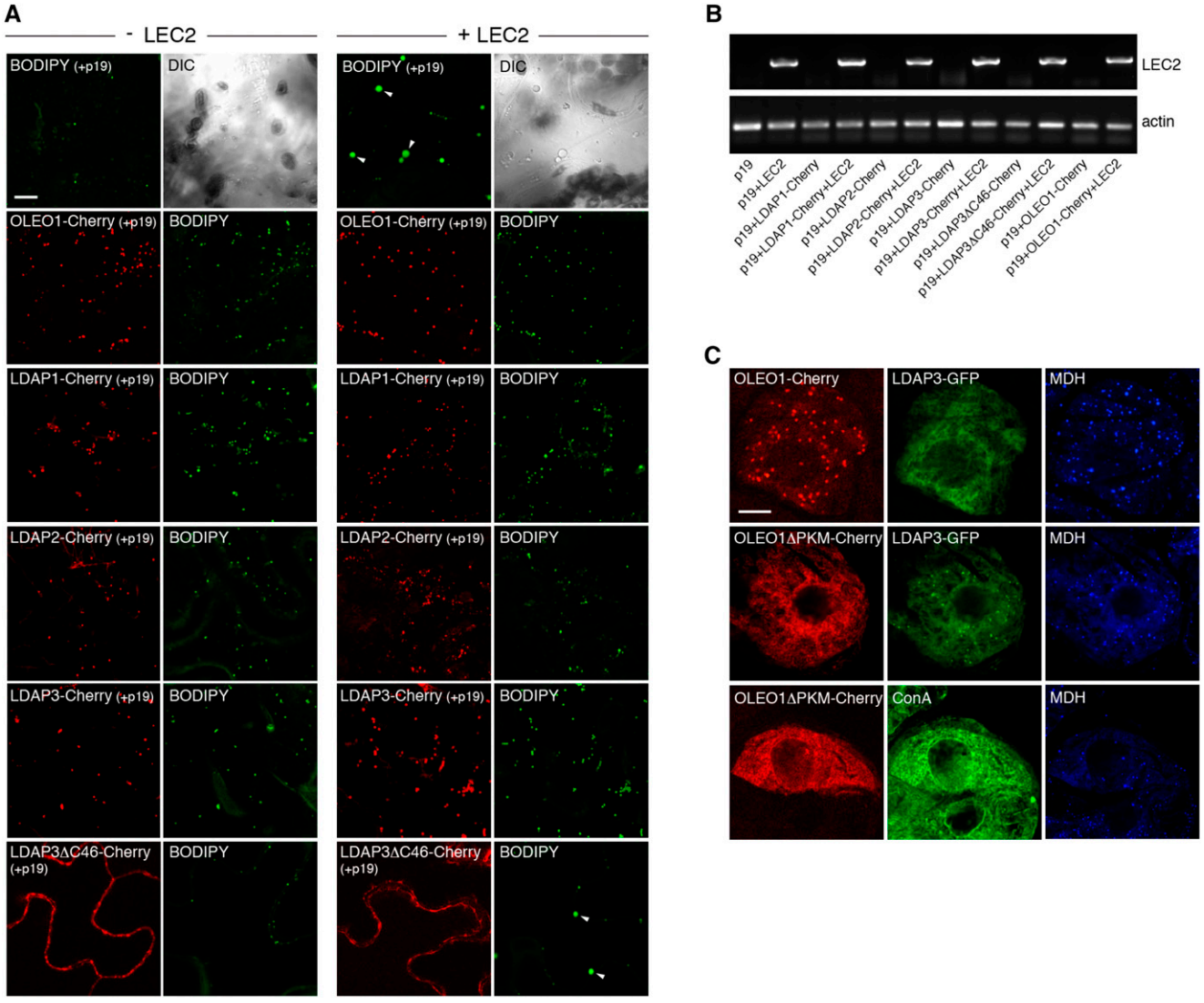

Figure 7. LDAPs and oleosin function similarly to compartmentalize lipids, but when ectopically expressed in the same cell, oleosin disrupts the binding of LDAP to LDs. A, Representative CLSM images of tobacco leaves transiently transformed with p19 (serving as a suppressor of gene silencing; Petrie et al., 2010) or p19 and either OLEO1-Cherry or LDAP-Cherry (or a modified version thereof) along with or without Arabidopsis LEC2, as indicated. LDs in all cells were stained with BODIPY. Note the presence of supersized LDs (indicated with arrowheads) in cells transformed with LEC2 and p19 (top row) or LEC2, p19, and LDAP3ΔC46-Cherry (bottom row), which does not target to LDs (Fig. 2A). By contrast, all cells coexpressing LEC2 (and p19) with either oleosin or an LDAP possess normal-sized LDs in comparison with controls without LEC2 (left images). DIC, Differential interference contrast. Bar = 20 μm. B, RT-PCR analysis of *LEC2* gene expression, confirming the presence of *LEC2* transcripts in all samples cotransformed with *LEC2*. ACTIN served as an endogenous control. C, Coexpression of oleosin and LDAP3 in tobacco cv BY-2 cells. Representative CLSM images show the localization of OLEO1-Cherry to MDH-stained LDs and the cytosolic (mis)localization of LDAP3-GFP in the same cell (top row; compare with images of oleosin and LDAP3 localized to LDs in individually transformed cv BY-2 cells in Fig. 2, A and B). By contrast, when LDAP3-GFP is coexpressed with the OLEO1-ΔPKM-Cherry mutant, which is retained in the ER (Abell et al., 1997; see also images in the bottom row), the localization of LDAP3-GFP to LDs in the same cell is enhanced (middle row). Bar = 10 μm.

These data confirm that both oleosin and LDAPs can function similarly to compartmentalize neutral lipids into normal-sized LDs.

To further characterize the functional properties of oleosin and LDAPs when present in the same cells, we coexpressed oleosin and LDAP3 in tobacco cv BY-2 cells. While each protein was able to target to LDs when expressed individually in cv BY-2 cells (Fig. 2B), coexpression of the two proteins resulted in oleosin association with LDs, whereas LDAP3 was localized primarily in the cytosol (Fig. 7C). On the other hand, coexpression of a mutant version of oleosin (i.e. OLEO1ΔPKM-Cherry), whereby the Pro knot motif (PKM) within the protein's hydrophobic region was disrupted, causing it to be trafficked more slowly to LDs via the ER (Abell et al., 1997), resulted in a prominent retention of oleosin in the ER and a greater proportion of LDAP3 associated with LDs (Fig. 7C). Taken together with the data presented in Figure 5, these observations support a model in plant seeds whereby oleosin, which is initially synthesized on the ER and trafficked to the surface of nascent LDs (Beaudoin and Napier, 2000, 2002), interferes with the association of LDAPs with LDs. However, once germination takes place, oleosins are degraded (Deruyffelaere et al., 2015), and as this proceeds, there is potential for a greater association of LDAPs with LDs, suggesting a previously unappreciated transition to an LDAP-mediated compartmentalization and regulation of TAG metabolism during postgerminative growth.

DISCUSSION

LDs are unique subcellular organelles that compartmentalize a variety of hydrophobic compounds in plants, including TAGs, steryl esters, and polyisoprenoids (Murphy, 2012; Khor et al., 2013). While the majority of our knowledge regarding the biogenesis and function of these organelles in plants comes from studies of oilseeds, there is increasing appreciation that LDs also play important and dynamic roles in a variety of other physiological processes within the vegetative tissues and organs of plants (Shimada et al., 2014, 2015; Shimada and Hara-Nishimura, 2015). Here, we characterized a family of proteins in Arabidopsis called LDAPs, which are related to the SRPP proteins in rubber-accumulating plants and which are known to coat the surface of LDs in nonseed cell types (Horn et al., 2013; Gidda et al., 2013; Divi et al., 2016). Overall, our studies reveal both shared and distinct properties of the three members of the Arabidopsis LDAP family and provide new avenues of research to explore LD dynamics and neutral lipid homeostasis in plants.

Targeting and Association of LDAPs with LDs in Vegetative Cell Types

All three Arabidopsis LDAPs targeted with high specificity to LDs in a variety of vegetative cell types (Fig. 1C; Supplemental Fig. S2), and when overexpressed in cv BY-2 cells lacking abundant LDs, they (mis)localized predominantly to the cytosol (Fig. 2; Supplemental Fig. S4A). This latter observation was somewhat surprising, since overexpression of membrane-associated proteins often results in their mistargeting to other organelle surfaces, such as the ER (Wagner et al., 2006). The high fidelity of LDAP targeting to LDs, therefore, raises intriguing questions regarding how these proteins can distinguish between various organelle surfaces within the cell. Notably, all of the LDAPs lack any apparent targeting signals or hydrophobic regions predicted for membrane association (Fig. 1A; Supplemental Fig. S1), and while comparisons of their polypeptide sequences revealed that they are all highly enriched in charged residues, particularly toward the N and C termini (Fig. 1A), their overall net charge varies considerably, ranging from +11 for LDAP1 and +4 for LDAP3 to −29 for LDAP2 (Supplemental Fig. S10). While it is currently unknown whether charge density is an important factor for LDAP targeting and/or function, these trends in charge density, including a net negative charge for LDAP2, are conspicuously conserved among LDAP members of other distantly related plant species (Supplemental Fig. S10).

Truncation analysis of LDAP3, serving as a candidate protein for studying the LDAP family, revealed that essentially the entire protein was required for targeting to LDs in vivo (Fig. 2A). This was somewhat unexpected, given that several discrete LD-targeting signals have been identified for LD proteins in a variety of organisms (DiNitto et al., 2003; Ingelmo-Torres et al., 2009; De Domenico et al., 2011). Furthermore, the REF protein of *H. brasiliensis*, which is similar in sequence to the N-terminal half of SRPP but lacks the corresponding C-terminal half, still effectively targets to and associates with rubber particles (Berthelot et al., 2012). Structural studies of REF and SRPP, however, suggest that the two rubber particle proteins adopt different conformations (Berthelot et al., 2012, 2014a) and thus may have evolved independent mechanisms for LD association. Regardless, we showed that progressive deletions of the C-terminal region of LDAP3 effectively abolished LD association in vivo (Fig. 2A); thus, it appears that the entire protein sequence is required for high-fidelity association with LDs. This is somewhat different from the results for SRPP, where studies have shown that deletion of the C-terminal half of the protein did not abolish a capability to interact with membranes (Berthelot et al., 2014c), although these studies were conducted using purified proteins and membranes in vitro and, thus, the observed differences might be due to the experimental approaches employed.

Investigations of LDAP interaction with LDs in vivo revealed that the association was sensitive to Triton X-100 but not digitonin (Fig. 2B), and given that these detergents differentially perturb lipids (Wolvetang et al., 1990; Lee et al., 1997; Jamur and Oliver, 2010), one explanation might be that protein-lipid interactions are important for LDAP targeting fidelity. However, incubation of LDAP3 with liposomes of various phospholipid compositions resulted in similar low-affinity binding (Fig. 2C; Table I). Thus, it is likely that additional factors, such as other

membrane-associated proteins or perhaps posttranslational modifications, are required for the proper targeting of LDAPs to the LD surface. Furthermore, given that the SRPP and REF proteins are known to self-associate and aggregate (Berthelot et al., 2014a), it is possible that once the LDAPs target to the surface of LDs, their local concentration would increase on the two-dimensional surface, thus promoting homotypic and heterotypic associations that might be important for coat formation.

The coexpression of oleosin and LDAPs in cv BY-2 cells resulted in oleosin targeting to LDs and LDAP remaining in the cytosol (Fig. 7C). These observations support a model whereby oleosin, which is known to be synthesized cotranslationally at the ER and then trafficked to LDs via the ER (Beaudoin and Napier, 2000, 2002), blocks the binding of LDAPs, which lack an obvious ER-targeting signal and thus likely target to LDs directly from the cytosol. This model also provides a potential mechanism for LD biogenesis in developing seeds, wherein the temporal and spatial synthesis of oleosins in embryos would result in primarily oleosin-coated LDs, which is well known to be important for maintaining LD integrity during seed desiccation (Huang, 1996; Hsieh and Huang, 2004). Once germination takes place and oleosins are degraded (Deruyffelaere et al., 2015), and perhaps the degree of protein crowding at the LD surface is reduced (Kory et al., 2015), LDAPs could begin to associate more readily with LDs from the cytosol, including with any nascent LDs that might carry out functions distinct from storage oil mobilization. Notably, all three LDAPs showed the capacity to bind to LDs 1 d after the initiation of germination (Fig. 5B), but disruption of *LDAP1* specifically, and not *LDAP2* or *LDAP3*, resulted in aberrant TAG packaging at this same stage (Fig. 6). Of course, this defect could be due to the stoichiometric reduction of total LDAPs in the cells rather than a distinct functional property of LDAP1, since the *LDAP1* gene is induced during seed imbibition (Fig. 1B). Regardless, the results illustrate that LDAPs play an important role in the transition from oleosin-coated LDs to LDAP compartmentalization during postgerminative growth and, furthermore, that loss of LD integrity is associated with reduced TAG turnover (Fig. 6A). This loss of LD integrity and reduction of LD-associated biochemical activities are similar to results observed for the suppression of SRPPs, which resulted in a destabilization of rubber particles and a reduction in associated polyisoprene biosynthesis (Hillebrand et al., 2012). Furthermore, reduction of oleosin proteins is known to result in aberrant LD formation, organellar instability, and fusions (Siloto et al., 2006; Miquel et al., 2014). It will be interesting, therefore, to continue to explore the mechanisms by which LDAPs associate with LDs and how proper compartmentalization of storage lipids is required to effectively engage the TAG degradation machinery in germinating seeds.

Modulation of LD Abundance and Neutral Lipid Homeostasis in Plant Leaves

In addition to modulating LD integrity during postgerminative growth, we also observed the effects of overexpression or suppression of LDAPs on modulating LD abundance in plant leaves (Fig. 3, B and C). In preliminary experiments using wild-type plants, we found that LD abundance varied considerably throughout the diurnal cycle, with the greatest number of LDs observed at the end of the night and fewer numbers seen throughout the day (Fig. 3A). Given that fatty acid biosynthesis generally requires reductant derived from photosynthesis (Chapman et al., 2013), the increase in LDs during the night is not likely due to de novo fatty acid synthesis. Instead, TAG and LDs likely increase due to membrane remodeling and recycling (Lin and Oliver, 2008; Chapman et al., 2013). Notably, growth and metabolism during the night are typically supported by the degradation of starch and sugars, but if plants encounter extended darkness, they can mobilize fatty acids for carbon and energy instead (Stitt and Zeeman, 2012; Weise et al., 2012). Perhaps this TAG reservoir is utilized in part for this purpose or remobilized during the day for the regeneration of appropriate organelles, depending on tissue/cell type, developmental stage, and/or physiological status of the cell. Surprisingly, suppression of any of the three LDAPs reduced the number of LDs observed at the end of the night (Fig. 3), suggesting that either each of the proteins performs distinct functions required for modulating LD abundance or, perhaps more likely, that a certain stoichiometric level of LDAP protein is required for proper LD biogenesis and maintenance. Alternatively, the reduction of LDAPs might confer greater susceptibility of the neutral lipid core of the LD to the degradation machinery, thereby decreasing the steady-state number of LDs in the cells. This does not appear to be the case, however, since total neutral lipid content in each LDAP suppression line was not reduced in comparison with the wild type (Fig. 3C).

Overexpression of LDAPs, on the other hand, resulted in both an increase in LDs as well as an increase in neutral lipid content of plant leaves (Fig. 3B). These data are somewhat similar to results from the overexpression of SEIPIN in plant cells (Cai et al., 2015). SEIPIN is a recently characterized ER-resident protein in plants that plays a critical and evolutionarily conserved role in the biogenesis of LDs at specific subdomains of the ER (Cartwright and Goodman, 2012; Cai et al., 2015). While SEIPIN is not involved directly in the biosynthesis of neutral lipids, per se, the promotion of LD biogenesis by this protein results in a steady-state increase in cellular neutral lipid content (Cai et al., 2015). These observations further suggest that the packaging of TAG into nascent LDs is rate limiting for determining neutral lipid accumulation. Similarly, overexpression of LDAPs might enhance or help to promote the process of LD formation and/or stabilization. For instance, the perilipin proteins in mammalian cells are thought to target in a posttranslational manner to subdomains of ER that are involved in LD biogenesis, prior to release of the LDs into the cytosol (Brasaemle et al., 1997; Jacquier et al., 2011). We have also observed a localization of LDAPs to LDs that are

associated with ER subdomains containing SEIPIN (Supplemental Fig. S11), although these data need to be substantiated using other approaches. Taken together, the results of our studies reveal that LDs are dynamically regulated throughout the diurnal cycle and that LDAPs play an important role in modulating their abundance. Additional studies are required to elucidate the physiological significance of this modulation, particularly in regard to carbon/energy balance and perhaps membrane recycling.

A Role for LDAPs during the Plant Stress Response

There is increasing and converging evidence that LDs play important roles during both biotic and abiotic stress responses in plants. For instance, the *LDAP* genes and their *SRPP* counterparts are strongly induced in some plants in response to abiotic stress (Sookmark et al., 2002; Priya et al., 2007; Kim et al., 2010; Seo et al., 2010; Fricke et al., 2013) as well as ectopic application of abscisic acid, as indicated by the Arabidopsis eFP Browser microarray database (Winter et al., 2007). LDs are also known to be involved in lipid metabolism associated with pathogen infection (Herker and Ott, 2012; Murphy, 2012), and biochemical studies have shown a significant increase in TAG and neutral lipids in plants subjected to heat, cold, drought, and salt stress (Mueller et al., 2015; Tarazona et al., 2015). LDs are also well known to be important in inflammatory responses in mammals (Melo and Weller, 2016). Taken together, it is likely that LD proliferation is a common cellular response during stress. Indeed, we showed that LDs increased nearly 10-fold in Arabidopsis leaves in response to either cold or heat stress (Fig. 4). The Arabidopsis *LDAP* genes, however, were differentially induced by stress, whereby, consistent with eFP Browser microarray results, *LDAP1* and *LDAP3* were both induced by cold but *LDAP1* alone was strongly induced by heat. Moreover, reduction of *LDAP3* expression resulted in reduced proliferation of LDs in response to cold (compared with the wild type), and loss of *LDAP1* resulted in fewer LDs in response to heat (Fig. 4). These data suggest that these LDAPs are particularly important for LD proliferation under each condition. But if the role of LDAPs is simply to compartmentalize storage lipids, why would different members of the family be selectively induced during abiotic stress? Indeed, why would there even be a need for three different LDAPs? One possibility is that, while each of the LDAPs does indeed function to compartmentalize lipids, they might interact differentially with other proteins and/or influence LDs in other ways that are important for the function(s) of the organelle in specific physiological contexts. For instance, while the perilipin proteins of mammals are known to be important for LD formation and maintenance, they also modulate lipid metabolism by interacting physically with proteins known to regulate TAG turnover (Lass et al., 2006). It is conceivable, therefore, that LDAPs function in a similar way in plants by interacting with and recruiting different sets of proteins to LDs, thus allowing LDs to participate in cellular metabolism in distinct ways depending on the physiological context. These questions could begin to be addressed by future protein interaction studies with LDAP isoforms. It is also interesting that the REF and SRRP proteins are thought to interact with components of the polyisoprene biosynthetic machinery to help promote rubber biosynthesis (Berthelot et al., 2014b).

The proliferation of LDs during environmental stress also has important implications for bioengineering strategies aimed at increasing the TAG (i.e. bioenergy) content of vegetative biomass. Recent studies by multiple groups, including our own, suggest that plants are remarkably amenable to an accumulation of elevated amounts of LDs and TAG in leaves (James et al., 2010; Fan et al., 2014; Vanhercke et al., 2014; Cai et al., 2015; Zale et al., 2016), thus providing a potential means for producing significantly higher amounts of biofuels in nonfood crop plants. Given the increasing evidence that LDs are likely to be important for the plant stress response, it will be important to determine how the directed proliferation of LDs will impact the adaptation of plants to environmental stress. It is conceivable that enhanced LD proliferation, which likely would incur other carbon/energy costs to the plant, could be involved in the remodeling of acyl groups for changes in membranes that may be required for plant tolerance to various stresses. In general, the studies described here provide a solid foundation to address these questions, which will further illuminate the role of the LDs in plant cells and possibly set the stage for more sustainable production of biofuels in crop plants.

MATERIALS AND METHODS

Plant Material, Growth Conditions, and Transformations

All Arabidopsis (*Arabidopsis thaliana*)-based experiments employed the wild-type Columbia-0 ecotype and derivatives thereof, including T-DNA insertional mutant lines (i.e. *ldap2-1* [SALK_099743], *ldap2-2* [SALK_060850], and *ldap1-1* [GABI-Kat 309G05]), obtained from the Arabidopsis Biological Resource Center (https://abrc.osu.edu) or GABI-Kat (https://www.gabi-kat.de; Kleinboelting et al., 2012), respectively, and transgenic lines either overexpressing or suppressing (via RNAi) selected *LDAP* genes. See below for details regarding overexpression and RNAi binary vector construction. Plants were stably transformed via *Agrobacterium tumefaciens* (strain GV3101) using the method of Clough and Bent (1998), and then progeny analysis was used to identify single-insertion, homozygous T3 plants. Genotyping and gene expression (or suppression) were evaluated in seedlings using PCR and RT-PCR, respectively (Supplemental Fig. S7), and two independent lines for each transgenic event were selected for further study. Arabidopsis plants were cultivated in soil in an environmental room with a 16-h/8-h day/night cycle at 22°C and 50 μE m^{-2} s^{-1} light intensity, or seeds were sterilized and plated on one-half-strength MS plates (Murashige and Skoog, 1962), then stratified for 3 d in the dark at 4°C before being moved into a growth chamber for the initiation of germination, with similar growth conditions to those described above. To analyze lipid degradation in seeds and seedlings, mature dry seeds and seedlings 1, 2, and 4 d after the initiation of germination were collected. Cold and heat stress experiments were carried out according to the procedures described by Mueller et al. (2015) and the Arabidopsis eFP Browser's abiotic stress data source (http://bar.utoronto.ca; Winter et al., 2007). Briefly, 15-d-old seedlings (at the end of the day period) were either maintained at normal (control) temperatures or transferred to either a 4°C or 37°C growth chamber and incubated for either 24 or 1 h, respectively, under a normal day/night cycle.

Nicotiana benthamiana plants used for *A. tumefaciens*-mediated transient expression experiments were grown in soil at 28°C with a 16-h/8-h day/night

cycle. Leaves of 4-week-old tobacco (*Nicotiana tabacum*) plants were infiltrated with *A. tumefaciens* (strain LBA4404 or GV3101) carrying selected binary vectors (see below for details on vector construction). *A. tumefaciens* transformed with the tomato bushy stunt virus gene *P19* was included in all infiltrations to enhance transgene expression (Petrie et al., 2010). LEC2 was included in selected infiltrations to enhance the synthesis of TAG and to simulate seed cellular physiology in *N. benthamiana* leaves (Petrie et al., 2010). Procedures for *A. tumefaciens* growth, transformation, infiltration, and processing of leaf material for microscopy (see below) have been described elsewhere (McCartney et al., 2005; Petrie et al., 2010; Cai et al., 2015).

Tobacco cv BY-2 suspension-cultured cells were maintained and prepared for biolistic bombardment as described previously (Lingard et al., 2008). Induction of LDs in cv BY-2 cells with LA-albumin conjugate (Sigma-Aldrich) and differential detergent permeabilization experiments with digitonin and Triton X-100 were performed according to Horn et al. (2013) and Lee et al. (1997), respectively.

Gene Cloning and Plasmid Construction

Molecular biology reagents were purchased from New England Biolabs, Promega, PerkinElmer Life Sciences, Stratagene, or Invitrogen, and custom oligonucleotides were synthesized by Sigma-Aldrich. Sequence information for all primers used in gene cloning and plasmid construction are available upon request. All DNA constructs were verified using automated sequencing performed at the University of Guelph Genomics Facility.

The coding regions of Arabidopsis *LDAP1* and *LDAP2* were cloned as described previously for *LDAP3* (Horn et al., 2013). Briefly, the full-length open reading frames (ORFs) of *LDAP1* and *LDAP2* were amplified using gene-specific forward and reverse primers and a complementary DNA library obtained from isolated Arabidopsis suspension-cultured cell mRNA as template. Resulting PCR products were digested with *Nhe*I and subcloned into *Nhe*I-digested pRTL2/Cherry, a plant transient expression vector containing the 35S cauliflower mosaic virus promoter, followed by a multiple cloning site (MCS) and the ORF of the monomerized red fluorescent protein Cherry (Gidda et al., 2011). Thereafter, the coding region for each LDAP-Cherry fusion protein was subcloned into the plant expression binary vector pMDC32 using Gateway technology (Curtis and Grossniklaus, 2003), and the resulting plasmids were used for either stable transformation of Arabidopsis or transient transformation of *N. benthamiana* leaves.

pRTL2 expression vectors encoding GFP-tagged versions of LDAP1, LDAP2, or LDAP3 used in transient transformation experiments with cv BY-2 cells were generated by amplifying (via PCR) each *LDAP* ORF from its respective pRTL2/LDAP-Cherry template, along with the appropriate primers. Thereafter, PCR products were digested and subcloned into pRTL2/mGFP-MCS, encoding the ORF of the monomerized GFP (mGFP), and/or pRLT2/*Nhe*I-mGFP, encoding mGFP with a 5′ unique *Nhe*I restriction site (Clark et al., 2009). Truncation mutants of LDAP3-GFP were generated using PCR-based site-directed mutagenesis and pRLT2/LDAP3-GFP as template DNA. Specifically, primers designed for introducing N- or C-terminal mutations in the LDAP3 coding region included either an *Nco*I restriction site, which contains a transitional initiation codon (underlined, CCATGG) or a stop codon followed by an *Xma*I restriction site, respectively. Following mutagenesis, the modified plasmids were digested with the corresponding restriction enzyme and religated. Similarly, the C-terminal LDAP3 truncation mutant, LDAP3-CherryΔC46, was generated using site-directed mutagenesis with pRTL2/LDAP3-Cherry as template, followed by subcloning of the coding sequence for LDAP3-CherryΔC46 into pMDC32 using Gateway technology.

Plant transient expression vectors encoding Arabidopsis OLEO1 were generated by amplifying the full-length OLEO1 ORF from pUNI51/OLEO1 (clone 115M7, obtained from the Arabidopsis Biological Resource Center) and subcloning the resulting PCR products into either pUC18/*Nco*I-mGFP, encoding mGFP with a unique 5′ *Nco*I restriction site (Clark et al., 2009), or pRTL2/Cherry. pRTL2/OLEO1ΔPKM-Cherry, encoding a previously characterized mutant version of oleosin, whereby the Pro residues at positions 83 and 87 in the PKM were replaced with Leu (Abell et al., 1997), was generated using PCR-based site-directed mutagenesis. The coding regions for OLEO1-Cherry and OLEO1ΔPKM-Cherry fusion proteins were then subcloned into pMDC32 using Gateway technology. Plant binary vectors encoding LEC2, a regulator of seed development (pORE04-LEC2), and the tomato bushy stunt virus RNA-silencing suppressor p19 (pORE04-P19) were kindly provided by Q. Liu (Petrie et al., 2010). pRTL2/GFP-DGAT2, encoding Arabidopsis DGAT2 linked to GFP at its N terminus, and pMDC84/SEIPIN1-GFP, encoding Arabidopsis SEIPIN isoform 1 fused to GFP, have been described previously (Shockey et al., 2006; Cai et al., 2015). pMDC32/Kar2-CFP-HDEL, encoding the cyan fluorescent protein (CFP) fused to the KARYOGAMY2 (Kar2) protein's N-terminal ER signal sequence and C-terminal HDEL ER retrieval signal, was constructed by PCR-amplifying sequences encoding the fusion protein along with the appropriate restriction sites from pRS316-Kar2-CFP-HDEL (Szymanski et al., 2007) and ligating into pMDC32 (Curtis and Grossniklaus, 2003).

The construction of *LDAP1*- and *LDAP3*-specific RNAi vectors was carried out by amplifying (via PCR) selected regions of the *LDAP1* or *LDAP3* genes (Supplemental Fig. S7) and subcloning the resulting PCR products into the Gateway vector pB7GW1WG2 (Karimi et al., 2002). For LDAP3 liposome-binding experiments, an *Escherichia coli* codon-optimized, single-Cys-containing version of the Arabidopsis LDAP3 ORF was custom synthesized by Integrated DNA Technologies. Specifically, the modified LDAP3 coding sequence encoded an Ala in place of the Cys at position 196 ($C^{196}A$), resulting in a single remaining Cys at position 168 being available for donor fluorophore labeling in FRET experiments (see below). The coding sequence for LDAP3 ($C^{196}A$) was subcloned into pET11a, yielding LDAP3 ($C^{196}A$) with N-terminal-appended poly(His) and Tobacco Etch Virus (TEV) tag sequences. Details on the plasmid encoding recombinant human BIM with a single Cys are provided elsewhere (Lovell et al., 2008)

RT-PCR

Assessment of *LDAP* gene expression at the transcriptional level in various tissues/organs in wild-type Arabidopsis (Columbia-0) and 15-d-old leaves from transgenic lines, including those used in abiotic stress experiments, was carried out using RT-PCR based on procedures described by Cai et al. (2015). Total RNA was purified from approximately 50 mg of plant material using the RNeasy Plant Mini Kit (Qiagen) and treated with DNase (Promega) to avoid DNA contamination. Complementary DNA was synthesized from total RNA using the qScript cDNA Super Mix, according to the manufacturer's instructions (Quanta Biosciences). *LDAP1*, *LDAP2*, and *LDAP3* were amplified by 30 cycles of 94°C for 30 s, 55°C for 30 s, and 72°C for 90 s. *EF1α* and *TUBULIN* were used as control genes expressed in nontransgenic and/or transgenic tissues and were amplified by 30 cycles of 94°C for 30 s, 55°C for 30 s, and 72°C for 1 min. For each reaction, 500 ng of total RNA was used. Specific forward and reverse primers for the amplification of *LDAP1*, *LDAP2*, *LDAP3*, and *EF1α* are provided in Supplemental Table S2.

RT-PCR to assess the expression of *LEC2* in *N. benthamiana* leaf tissue was also carried out according to Cai et al. (2015): *LEC2* and *ACTIN*, serving as a control gene, were amplified by 35 cycles of 94°C for 30 s, 50°C for 30 s, and 72°C for 1 min using gene-specific forward and reverse primers (Supplemental Table S2).

Microscopy

Wild-type and transgenic Arabidopsis seedlings and *A. tumefaciens*-infiltrated tobacco leaves were processed for CLSM imaging, including staining of LDs, as described previously (Park et al., 2013; Cai et al., 2015). Arabidopsis dry seeds were imbibed in water for 15 min to soften the seed coat, and seed coats were removed from both dry seeds and germinating seeds by rolling embryos out of seed coats under a coverslip. Embryos were stained with BODIPY 493/503 (Invitrogen) in 50 mM PIPES buffer (pH 7) for 20 min followed by three washes with 50 mM PIPES buffer (10 min each time). Thereafter, embryos were mounted with deionized water on slides for imaging. The cv BY-2 cells were incubated (with or without LA) for 4 to 8 h following biolistic bombardment, fixed in paraformaldehyde (Electron Microscopy Sciences), permeabilized according to Lee et al. (1997) and Lingard et al. (2008), and then incubated with the appropriate LD stain (see below).

Microscopic images of stably transformed 15-d-old Arabidopsis seedlings and transiently transformed tobacco leaves, as well as transiently transformed cv BY-2 cells (besides those stained with MDH; see below), were acquired using a Leica DM RBE microscope with a Leica 63× Plan Apochromat oil-immersion objective, a Leica TCS SP2 scanning head, and the Leica TCS NT software package. CLSM images of Arabidopsis dry seeds and seedlings following the initiation of germination, as well tobacco leaves in LDAP3-SEIPIN1 coexpression experiments (Supplemental Fig. S12), were acquired using a Zeiss LSM710 confocal laser-scanning microscope. MDH-stained cv BY-2 cells were imaged using the Leica SP5 CLSM system equipped with a Radius 405-nm laser. BODIPY 493/503, a green fluorescent neutral lipid stain (Listenberger et al., 2007), GFP, and chlorophyll autofluorescence were excited with a 488-nm laser, Cherry and Nile Red with a 543-nm laser, and CFP and MDH with a 405-nm laser. Emission fluorescence signals were collected as follows: 500 to 540 nm for BODIPY and GFP, 650 to 757 for chlorophyll, 590 to 640 nm for Cherry and Nile Red, 450 to 490 for CFP, and 420 to 480 for MDH. LDs were stained with 2 μg mL^{-1} BODIPY (for Arabidopsis and tobacco leaves; from 4 mg mL^{-1} stock in

dimethyl sulfoxide [DMSO]), 2 μg mL^{-1} Nile Red (for tobacco leaves [Sigma-Aldrich]; from 1 mg mL^{-1} stock in DMSO) in 50 mM PIPES buffer (pH 7), or 0.1 μg mL^{-1} BODIPY or 0.3 μM MDH (a blue fluorescent neutral lipid stain [Yang et al., 2012b]; for cv BY-2 cells [Abgent]; from 100 μM stock in DMSO) in phosphate-buffered saline (pH 7). All fluorophore emissions were collected sequentially in double- or triple-labeling experiments; single-labeling experiments showed no detectable crossover at the settings used for data collection. Images were acquired as individual single optical sections or as a Z-series, and, depending on the CLSM system employed, sections were saved as either 512- × 512-pixel or 1,024- × 1,024-pixel digital images. All fluorescence images of cells shown in individual figures are representative of at least two separate experiments, including at least 25 independent (transient) transformations of tobacco leaf and cv BY-2 cells. Arabidopsis seedlings were fixed and processed for transmission electron microscopy as described previously (Cai et al., 2015), and images were collected using a Philips EM420 transmission electron microscope. All figure compositions were generated using Adobe Photoshop CS and Illustrator CS2 (Adobe Systems).

LD Quantification

The number of LDs in leaves of 15-d-old Arabidopsis seedlings was quantified according to Cai et al. (2015) using the Analyze Particles function at ImageJ (version 1.43; http://rsbweb.nih.gov/ij/docs/guide/146-30.html). Eight Z-stack series projections from three individual experiments for the wild type and each *LDAP* transgenic (overexpression or suppression) line (Fig. 3), light/dark treatment (Supplemental Fig. S6), or abiotic stress condition (Fig. 4) were used to quantify the number of BODIPY-stained LDs. The third or fourth leaf from the bottom of each Arabidopsis seedling was used for LD visualization and quantification. For quantification of BODIPY-stained LDs in cv BY-2 cells treated with or without LA (Supplemental Fig. S3), Z-stack projections of individual cells were assessed as 8- × 8-μm^2 regions. Overall, more than 100 areas within the cytosol of at least 25 cells from both LA-induced and uninduced conditions and from at least three separate experiments were analyzed. All the significance assessments in this study were performed using Student's *t* test.

Liposome-Binding Assays

The LDAP3 (C^{196}A) recombinant protein was expressed in *E. coli* and purified by chromatography on nickel resin followed by cobalt resin using standard methods. BIM protein purification will be published elsewhere (X. Chi and D.W. Andrews, unpublished data). *E. coli* GroEL was purified based on it copurifying with the recombinant LDAP3 protein on nickel-affinity resin; the identity of GroEL was confirmed by amino acid sequencing of the protein's N terminus. All proteins were labeled with Alexa-568-maleimide (Invitrogen) and LDAP3 (C^{196}A), and GroEL were then separated by a final chromatography step on cobalt-affinity resin, as His-tagged LDAP3 (C^{196}A) bound to the cobalt beads but GroEL did not (Supplemental Fig. S5).

Unilamellar 100-nm liposomes with different lipid compositions, based on phospholipid ratios for LDs (P.J. Horn and K.D. Chapman, unpublished data), ER and plasma membrane (Brown and Dupont 1989), and mitochondria (Lovell et al., 2008), were prepared by extrusion as described by Shamas-Din et al. (2015) and labeled with the acceptor dye DiD (Invitrogen). To assay protein binding to membranes, FRET was measured using a Tecan M1000 Pro microplate reader (Tecan Photon Technology International) using excitation at 578 nm and measuring the decrease in donor fluorescence at 603 nm when DiD-labeled liposomes were added to the protein in assay buffer (10 mM HEPES, pH 7, 0.2 M KCl, 5 mM $MgCl_2$, and 0.2 mM EDTA) at 25°C (Lovell et al., 2008). Samples were assayed in duplicate for final concentrations of liposomes from 0 to 3 nM. Unlabeled liposomes served as a negative control. Liposomes and proteins were warmed to 25°C before mixing, and 2 h after mixing, the fluorescence of the donor was recorded for 10 min. In each experiment, data from two replicates were averaged, background signals between labeled protein and unlabeled liposome were subtracted, and any signal from random collisions between dyes was adjusted based on the signal detected between free Alexa-568 dye and liposomes. The data presented for all liposome-binding assays are averages from at least three independent experiments.

Analysis of Plant Lipids

For thin-layer chromatography analysis of lipids from plant leaves, 15-d-old Arabidopsis seedlings grown on one-half-strength MS medium under 16-h/8-h light (50 μE m^{-2} s^{-1})/dark cycles were harvested at the end of the light cycle for overexpression lines and at the end of the dark cycle for T-DNA and RNAi mutant lines. Fresh weight was recorded, and then tissues were snap frozen in liquid nitrogen and stored at −80°C. Total lipids were extracted from the tissue using a hexane/isopropanol method (Hara and Radin, 1978). Briefly, approximately 500 mg of the frozen tissue was transferred into a 15-mL hand-held glass tissue grinder (Wheaton) containing 2 mL of hot isopropanol and incubated at 75°C for 15 min. After the sample was cooled down to room temperature, 3 mL of hexane was added and the tissue was homogenized. The homogenate was transferred into a clean glass tube. The homogenizer was rinsed once with 2 mL of 3:2 (v/v) hexane:isopropanol and combined with a homogenate. Three milliliters of 3.3% (w/v) Na_2SO_4 was added to the homogenate. Samples were shaken, vortexed, and centrifuged. The top organic phase was transferred to a clean glass tube, and lipids were reextracted once from the bottom aqueous phase with 3 mL of 7:2 (v/v) hexane:isopropanol and combined. The lipid extracts in hexane were dried down under a gentle stream of nitrogen and resuspended in chloroform, to result in a concentration of total lipids of 250 mg of tissue fresh weight per 30 μL of chloroform. Total lipid extracts were stored at 4°C until ready to analyze (1–2 d). Thirty-six microliters of the total lipid extracts (total lipids from 300 mg of tissue fresh weight) along with a TAG standard were applied on a silica thin-layer chromatography plate and developed in hexane:diethyl ether:acetic acid (70:30:1, v/v/v). Lipids were stained with 0.05% primuline in 80% acetone and visualized under UV light.

For fatty acid analysis in plant leaves, lipids were extracted from 15-d-old Arabidopsis seedlings following the same procedure as described above with 20 μg of C17:0 TAG (Sigma-Aldrich) internal standard added to the sample before tissue homogenization. Total lipid extracts were resuspended in 2 mL of hexane and separated into lipid classes on solid-phase extraction cartridges (Supelco Discovery DSC-Si 6 mL). After conditioning the cartridge with hexane and sample application, neutral lipids were eluted with 5 mL of hexane:diethyl ether (4:1, v/v). Chlorophyll was eluted with 5 mL of 1:1 (v/v) hexane:diethyl ether, and polar lipids were eluted with 5 mL of methanol and 3 mL of chloroform. The neutral lipid fraction was dried down under a gentle stream of nitrogen. One milliliter of 1.25 N HCl in methanol and 0.3 mL of toluene were added to the neutral lipids. Samples were vortexed and incubated at 85°C for 2 h. After the samples cooled down to room temperature, 1 mL of 0.9% NaCl was added to quench the reaction, and fatty acid methyl esters (FAMEs) were extracted with 1 mL of hexane. FAME samples were analyzed on the Agilent HP 6890 series gas chromatography system equipped with the 7683 series injector and autosampler. FAME samples were injected on a BPX70 (SGE Analytical Science) capillary column (10 m × 0.1 mm × 0.2 μm) with a 50:1 split ratio and separated with constant pressure of 25 p.s.i. and the following temperature program: hold at 140°C for 5 min, 140°C to 200°C at 4°C min^{-1}, hold at 200°C for 1 min, and 200°C to 250°C at 25°C min^{-1}. Integration events were detected between 9 and 20 min and identified by comparing with the GLC-10 FAME standard mix (Sigma-Aldrich).

To analyze lipid degradation in seeds during germination, sterilized seeds were sown on one-half-strength MS plates without Suc. Seeds on plates were stratified in the dark at 4°C for 3 d prior to being transferred to a growth room (22°C). Seeds were first exposed to light (100 μE m^{-2} s^{-1}) for 6 h and then kept in the dark in the growth room. Seeds were collected at 1, 2, and 4 d after the initiation of germination for lipid analysis. Approximately 50 dry seeds or germinating seeds were used for each biological replicate, and 50 μg of C17:0 TAG was spiked in each sample as an internal standard at the time of lipid extraction. Seeds were homogenized with glass beads, and lipid was extracted with 2 mL of isopropanol and 1 mL of chloroform at 70°C for 30 min followed by overnight incubation at 4°C. The lipid extract was further cleaned using 1 M potassium chloride three times. To quantify total lipid on a fatty acid basis, purified lipid was transesterified in 1 N methanolic HCl at 85°C for 2 h. FAMEs were dissolved in hexane and quantified by gas chromatography and flame ionization detection (Agilent HP 5890) with 25 p.s.i. pressure and the following temperature program: 180°C for 3 min, 180°C to 250°C at 5°C min^{-1}, and 250°C for 10 min.

Phylogenetic Analysis

The polypeptide sequences of various LDAP proteins were identified using the Protein Homologs tool available at Phytozome.net (database version 9.1; www.phytozome.net; Goodstein et al., 2012). Briefly, the Arabidopsis LDAP1 polypeptide sequence was used to identify LDAP isoforms in other plant species using the Protein Homologs tool available at Phytozome.net (database version 9.1; www.phytozome.net; Goodstein et al., 2012). The phylogenetic relationships of the resulting polypeptide sequences in each plant species shown in Supplemental Figure S10 were subsequently analyzed using the one-click Web interface available at phylogeny.fr, using default settings (http://www.phylogeny.fr; Dereeper et al., 2008, 2010).

Arabidopsis LDAP nomenclature was assigned based on chromosome locations of the respective genes: *LDAP1* (The Arabidopsis Information Resource no. At1g67360), GenBank accession no. NP_176904; *LDAP2* (At2g47780), NP_182299; and *LDAP3* (At3g05500), NP_187201. Additional genes described in this study include human *BIM* (O43521); Arabidopsis *DGAT2* (At3g51520), NP_566952; Arabidopsis *EF1α* (At1g07930), NP_200847; *Saccharomyces cerevisiae KAR2*, CAA89325.1; Arabidopsis *OLEO1* (At4g25140), NP_194244; Arabidopsis *α-TUBULIN* (At5g44340), NM_123801; Arabidopsis *SEIPIN1* (At5g16460), AED92296; *E. coli GroEL* (1407243B); and *N. benthamiana ACTIN*, AY179605. For Supplemental Figure S11, the LDAPs analyzed included were as follows: *Ricinus communis* Rco-LDAP1, XP_002514917; Rco-LDAP2, XP_002531884; Rco-LDAP3, XP_002512427; *Prunus persica* Ppe-LDAP1, XP_007223862; Ppe-LDAP2, XP_007201256; Ppe-LDAP3, XP_007205771; and *Solanum lycopersicum* Sly-LDAP1, XP_004239210; Sly-LDAP2, XP_004247432; and Sly-LDAP3, XP_004230235.

Supplemental Data

The following supplemental materials are available.

Supplemental Figure S1. Prediction of transmembrane-spanning domains in Arabidopsis LDAPs and oleosin.

Supplemental Figure S2. LDAP2 and LDAP3 localization in various vegetative cell types of 15-d-old Arabidopsis seedlings.

Supplemental Figure S3. Fatty-acid induced proliferation of LDs in tobacco BY-2 cells.

Supplemental Figure S4. Localization of LDAPs in tobacco BY-2 cells.

Supplemental Figure S5. Expression purification of recombinant LDAP3 protein from bacteria.

Supplemental Figure S6. LDAP gene expression and LD abundance in Arabidopsis leaves.

Supplemental Figure S7. Generation and characterization of LDAP overexpression and suppression transgenic Arabidopsis lines.

Supplemental Figure S8. Thin-layer chromatography analysis of total lipids extracted from Arabidopsis leaves.

Supplemental Figure S9. TEM of LDs in cotyledonary cells of wild-type and ldap mutant embryos.

Supplemental Figure S10. Phylogenetic tree and comparison of amino acid charge density in LDAPs from various plant species.

Supplemental Figure S11. Localization of LDAP3 and SEIPIN coexpressed in tobacco leaves.

Supplemental Table S1. Phospholipid composition of synthetic liposomes.

Supplemental Table S2. Synthetic oligonucleotide sequences used for RT-PCR and genotyping.

ACKNOWLEDGMENTS

We thank Dr. Qing Liu (Commonwealth Scientific and Industrial Research Organization Plant Industry) for pORE04-LEC2 and pORE04-P19, Dr. Patrick Horn (Michigan State University) for providing details on the phospholipid composition of avocado mesocarp LDs, Thuy Nguyen (University of Guelph) for assistance with LD quantifications, Dr. Xiaoke Chi (Sunnybrook Research Institute) for providing purified BIM protein used in liposome-binding experiments, Bob Harris (University of Guelph Imaging Facility) for assistance with electron microscopy, and Jamie Vulgamore, Maria Predtechenskaya (U.S. Department of Agriculture), and Ray De Villa (University of Guelph) for excellent technical assistance.

Received December 18, 2015; accepted February 18, 2016; published February 19, 2016.

LITERATURE CITED

Abell BM, Hahn M, Holbrook LA, Moloney MM (2004) Membrane topology and sequence requirements for oil body targeting of oleosin. Plant J **37:** 461–470

Abell BM, Holbrook LA, Abenes M, Murphy DJ, Hills MJ, Moloney MM (1997) Role of the proline knot motif in oleosin endoplasmic reticulum topology and oil body targeting. Plant Cell **9:** 1481–1493

Andrianov V, Borisjuk N, Pogrebnyak N, Brinker A, Dixon J, Spitsin S, Flynn J, Matyszczuk P, Andryszak K, Laurelli M, et al (2010) Tobacco as a production platform for biofuel: overexpression of Arabidopsis DGAT and LEC2 genes increases accumulation and shifts the composition of lipids in green biomass. Plant Biotechnol J **8:** 277–287

Beaudoin F, Napier JA (2000) The targeting and accumulation of ectopically expressed oleosin in non-seed tissues of *Arabidopsis thaliana*. Planta **210:** 439–445

Beaudoin F, Napier JA (2002) Targeting and membrane-insertion of a sunflower oleosin in vitro and in *Saccharomyces cerevisiae*: the central hydrophobic domain contains more than one signal sequence, and directs oleosin insertion into the endoplasmic reticulum membrane using a signal anchor sequence mechanism. Planta **215:** 293–303

Berthelot K, Lecomte S, Estevez Y, Coulary-Salin B, Bentaleb A, Cullin C, Deffieux A, Peruch F (2012) Rubber elongation factor (REF), a major allergen component in *Hevea brasiliensis* latex has amyloid properties. PLoS ONE **7:** e48065

Berthelot K, Lecomte S, Estevez Y, Coulary-Salin B, Peruch F (2014a) Homologous *Hevea brasiliensis* REF (Hevb1) and SRPP (Hevb3) present different auto-assembling. Biochim Biophys Acta **1844:** 473–485

Berthelot K, Lecomte S, Estevez Y, Peruch F (2014b) *Hevea brasiliensis* REF (Hev b 1) and SRPP (Hev b 3): an overview on rubber particle proteins. Biochimie **106:** 1–9

Berthelot K, Lecomte S, Estevez Y, Zhendre V, Henry S, Thévenot J, Dufourc EJ, Alves ID, Peruch F (2014c) Rubber particle proteins, HbREF and HbSRPP, show different interactions with model membranes. Biochim Biophys Acta **1838:** 287–299

Bewley JD (1997) Seed germination and dormancy. Plant Cell **9:** 1055–1066

Brandizzi F, Irons S, Kearns A, Hawes C (2003) BY-2 cells: culture and transformation for live cell imaging. Curr Protoc Cell Biol **Chapter 1:** Unit 1.7

Brasaemle DL, Barber T, Kimmel AR, Londos C (1997) Post-translational regulation of perilipin expression: stabilization by stored intracellular neutral lipids. J Biol Chem **272:** 9378–9387

Brown DJ, Dupont FM (1989) Lipid composition of plasma membranes and endomembranes prepared from roots of barley (*Hordeum vulgare* L.): effects of salt. Plant Physiol **90:** 955–961

Cai Y, Goodman JM, Pyc M, Mullen RT, Dyer JM, Chapman KD (2015) *Arabidopsis* SEIPIN proteins modulate triacylglycerol accumulation and influence lipid droplet proliferation. Plant Cell **27:** 2616–2636

Cartwright BR, Goodman JM (2012) Seipin: from human disease to molecular mechanism. J Lipid Res **53:** 1042–1055

Chapman KD, Dyer JM, Mullen RT (2012) Biogenesis and functions of lipid droplets in plants. J Lipid Res **53:** 215–226

Chapman KD, Dyer JM, Mullen RT (2013) Commentary: why don't plant leaves get fat? Plant Sci **207:** 128–134

Clark SM, Di Leo R, Dhanoa PK, Van Cauwenberghe OR, Mullen RT, Shelp BJ (2009) Biochemical characterization, mitochondrial localization, expression, and potential functions for an Arabidopsis gamma-aminobutyrate transaminase that utilizes both pyruvate and glyoxylate. J Exp Bot **60:** 1743–1757

Clough SJ, Bent AF (1998) Floral dip: a simplified method for Agrobacterium-mediated transformation of *Arabidopsis thaliana*. Plant J **16:** 735–743

Curtis MD, Grossniklaus U (2003) A Gateway cloning vector set for high-throughput functional analysis of genes in planta. Plant Physiol **133:** 462–469

De Domenico S, Bonsegna S, Lenucci MS, Poltronieri P, Di Sansebastiano GP, Santino A (2011) Localization of seed oil body proteins in tobacco protoplasts reveals specific mechanisms of protein targeting to leaf lipid droplets. J Integr Plant Biol **53:** 858–868

Dereeper A, Audic S, Claverie JM, Blanc G (2010) BLAST-EXPLORER helps you building datasets for phylogenetic analysis. BMC Evol Biol **10:** 8

Dereeper A, Guignon V, Blanc G, Audic S, Buffet S, Chevenet F, Dufayard JF, Guindon S, Lefort V, Lescot M, et al (2008) Phylogeny.fr: robust phylogenetic analysis for the non-specialist. Nucleic Acids Res **36:** W465–W469

Deruyffelaere C, Bouchez I, Morin H, Guillot A, Miquel M, Froissard M, Chardot T, D'Andrea S (2015) Ubiquitin-mediated proteasomal

degradation of oleosins is involved in oil body mobilization during post-germinative seedling growth in *Arabidopsis*. Plant Cell Physiol **56:** 1374–1387

DiNitto JP, Cronin TC, Lambright DG (2003) Membrane recognition and targeting by lipid-binding domains. Sci STKE **2003:** re16

Divi UK, Zhou XR, Wang P, Butlin J, Zhang DM, Liu Q, Vanhercke T, Petrie JR, Talbot M, White RG, et al (2016) Deep sequencing of the fruit transcriptome and lipid accumulation in a non-seed tissue of Chinese tallow, a potential biofuel crop. Plant Cell Physiol **57:** 125–137

Farese RV Jr, Walther TC (2009) Lipid droplets finally get a little R-E-S-P-E-C-T. Cell **139:** 855–860

Feeney M, Frigerio L, Cui Y, Menassa R (2013) Following vegetative to embryonic cellular changes in leaves of Arabidopsis overexpressing LEAFY COTYLEDON2. Plant Physiol **162:** 1881–1896

Fricke J, Hillebrand A, Twyman RM, Prüfer D, Schulze Gronover C (2013) Abscisic acid-dependent regulation of small rubber particle protein gene expression in *Taraxacum brevicorniculatum* is mediated by TbbZIP1. Plant Cell Physiol **54:** 448–464

Gidda SK, Shockey JM, Falcone M, Kim PK, Rothstein SJ, Andrews DW, Dyer JM, Mullen RT (2011) Hydrophobic-domain-dependent protein-protein interactions mediate the localization of GPAT enzymes to ER subdomains. Traffic **12:** 452–472

Gidda SK, Watt S, Collins-Silva J, Kilaru A, Arondel V, Yurchenko O, Horn PJ, James CN, Shintani D, Ohlrogge JB, et al (2013) Lipid droplet-associated proteins (LDAPs) are involved in the compartmentalization of lipophilic compounds in plant cells. Plant Signal Behav **8:** e27141

Goodstein DM, Shu S, Howson R, Neupane R, Hayes RD, Fazo J, Mitros T, Dirks W, Hellsten U, Putnam N, et al (2012) Phytozome: a comparative platform for green plant genomics. Nucleic Acids Res **40:** D1178–D1186

Greenberg AS, Egan JJ, Wek SA, Garty NB, Blanchette-Mackie EJ, Londos C (1991) Perilipin, a major hormonally regulated adipocyte-specific phosphoprotein associated with the periphery of lipid storage droplets. J Biol Chem **266:** 11341–11346

Hara A, Radin NS (1978) Lipid extraction of tissues with a low-toxicity solvent. Anal Biochem **90:** 420–426

Herker E, Ott M (2012) Emerging role of lipid droplets in host/pathogen interactions. J Biol Chem **287:** 2280–2287

Hillebrand A, Post JJ, Wurbs D, Wahler D, Lenders M, Krzyzanek V, Prüfer D, Gronover CS (2012) Down-regulation of small rubber particle protein expression affects integrity of rubber particles and rubber content in *Taraxacum brevicorniculatum*. PLoS ONE **7:** e41874

Horn PJ, James CN, Gidda SK, Kilaru A, Dyer JM, Mullen RT, Ohlrogge JB, Chapman KD (2013) Identification of a new class of lipid droplet-associated proteins in plants. Plant Physiol **162:** 1926–1936

Hsieh K, Huang AH (2004) Endoplasmic reticulum, oleosins, and oils in seeds and tapetum cells. Plant Physiol **136:** 3427–3434

Huang AH (1996) Oleosins and oil bodies in seeds and other organs. Plant Physiol **110:** 1055–1061

Ingelmo-Torres M, González-Moreno E, Kassan A, Hanzal-Bayer M, Tebar F, Herms A, Grewal T, Hancock JF, Enrich C, Bosch M, et al (2009) Hydrophobic and basic domains target proteins to lipid droplets. Traffic **10:** 1785–1801

Jacquier N, Choudhary V, Mari M, Toulmay A, Reggiori F, Schneiter R (2011) Lipid droplets are functionally connected to the endoplasmic reticulum in *Saccharomyces cerevisiae*. J Cell Sci **124:** 2424–2437

Jacquier N, Mishra S, Choudhary V, Schneiter R (2013) Expression of oleosin and perilipins in yeast promotes formation of lipid droplets from the endoplasmic reticulum. J Cell Sci **126:** 5198–5209

James CN, Horn PJ, Case CR, Gidda SK, Zhang D, Mullen RT, Dyer JM, Anderson RG, Chapman KD (2010) Disruption of the Arabidopsis CGI-58 homologue produces Chanarin-Dorfman-like lipid droplet accumulation in plants. Proc Natl Acad Sci USA **107:** 17833–17838

Jamur MC, Oliver C (2010) Permeabilization of cell membranes. Methods Mol Biol **588:** 63–66

Karimi M, Inzé D, Depicker A (2002) GATEWAY vectors for *Agrobacterium*-mediated plant transformation. Trends Plant Sci **7:** 193–195

Khor VK, Shen WJ, Kraemer FB (2013) Lipid droplet metabolism. Curr Opin Clin Nutr Metab Care **16:** 632–637

Kim EY, Seo YS, Lee H, Kim WT (2010) Constitutive expression of CaSRP1, a hot pepper small rubber particle protein homolog, resulted in fast growth and improved drought tolerance in transgenic Arabidopsis plants. Planta **232:** 71–83

Kim HU, Jung SJ, Lee KR, Kim EH, Lee SM, Roh KH, Kim JB (2013) Ectopic overexpression of castor bean LEAFY COTYLEDON2 (LEC2) in Arabidopsis triggers the expression of genes that encode regulators of seed maturation and oil body proteins in vegetative tissues. FEBS Open Bio **4:** 25–32

Kleinboelting N, Huep G, Kloetgen A, Viehoever P, Weisshaar B (2012) GABI-Kat SimpleSearch: new features of the *Arabidopsis thaliana* T-DNA mutant database. Nucleic Acids Res **40:** D1211–D1215

Kory N, Thiam AR, Farese RV Jr, Walther TC (2015) Protein crowding is a determinant of lipid droplet protein composition. Dev Cell **34:** 351–363

Laibach N, Post J, Twyman RM, Gronover CS, Prüfer D (2015) The characteristics and potential applications of structural lipid droplet proteins in plants. J Biotechnol **201:** 15–27

Lass A, Zimmermann R, Haemmerle G, Riederer M, Schoiswohl G, Schweiger M, Kienesberger P, Strauss JG, Gorkiewicz G, Zechner R (2006) Adipose triglyceride lipase-mediated lipolysis of cellular fat stores is activated by CGI-58 and defective in Chanarin-Dorfman syndrome. Cell Metab **3:** 309–319

Lee MS, Mullen RT, Trelease RN (1997) Oilseed isocitrate lyases lacking their essential type 1 peroxisomal targeting signal are piggybacked to glyoxysomes. Plant Cell **9:** 185–197

Levesque-Lemay M, Chabot D, Hubbard K, Chan JK, Miller S, Robert LS (2016) Tapetal oleosins play an essential role in tapetosome formation and protein relocation to the pollen coat. New Phytol **209:** 691–704

Lin WL, Oliver DJ (2008) Role of triacylglycerols in leaves. Plant Sci **175:** 233–237

Lingard MJ, Gidda SK, Bingham S, Rothstein SJ, Mullen RT, Trelease RN (2008) *Arabidopsis* PEROXIN11c-e, FISSION1b, and DYNAMIN-RELATED PROTEIN3A cooperate in cell cycle-associated replication of peroxisomes. Plant Cell **20:** 1567–1585

Listenberger LL, Ostermeyer-Fay AG, Goldberg EB, Brown WJ, Brown DA (2007) Adipocyte differentiation-related protein reduces the lipid droplet association of adipose triglyceride lipase and slows triacylglycerol turnover. J Lipid Res **48:** 2751–2761

Lovell JF, Billen LP, Bindner S, Shamas-Din A, Fradin C, Leber B, Andrews DW (2008) Membrane binding by tBid initiates an ordered series of events culminating in membrane permeabilization by Bax. Cell **135:** 1074–1084

McCartney AW, Greenwood JS, Fabian MR, White KA, Mullen RT (2005) Localization of the tomato bushy stunt virus replication protein p33 reveals a peroxisome-to-endoplasmic reticulum sorting pathway. Plant Cell **17:** 3513–3531

Melo RC, Weller PF (2016) Lipid droplets in leukocytes: organelles linked to inflammatory responses. Exp Cell Res **340:** 193–197

Miquel M, Trigui G, d'Andréa S, Kelemen Z, Baud S, Berger A, Deruyffelaere C, Trubuil A, Lepiniec L, Dubreucq B (2014) Specialization of oleosins in oil body dynamics during seed development in Arabidopsis seeds. Plant Physiol **164:** 1866–1878

Moellering ER, Benning C (2010) RNA interference silencing of a major lipid droplet protein affects lipid droplet size in Chlamydomonas reinhardtii. Eukaryot Cell **9:** 97–106

Mueller SP, Krause DM, Mueller MJ, Fekete A (2015) Accumulation of extra-chloroplastic triacylglycerols in Arabidopsis seedlings during heat acclimation. J Exp Bot **66:** 4517–4526

Murashige T, Skoog F (1962) A revised medium for rapid growth and bioassays with tobacco tissue cultures. Plant Physiol **15:** 473–497

Murphy DJ (2012) The dynamic roles of intracellular lipid droplets: from archaea to mammals. Protoplasma **249:** 541–585

Park S, Gidda SK, James CN, Horn PJ, Khuu N, Seay DC, Keereetaweep J, Chapman KD, Mullen RT, Dyer JM (2013) The α/β hydrolase CGI-58 and peroxisomal transport protein PXA1 coregulate lipid homeostasis and signaling in *Arabidopsis*. Plant Cell **25:** 1726–1739

Petrie JR, Shrestha P, Liu Q, Mansour MP, Wood CC, Zhou XR, Nichols PD, Green AG, Singh SP (2010) Rapid expression of transgenes driven by seed-specific constructs in leaf tissue: DHA production. Plant Methods **6:** 8

Priya P, Venkatachalam P, Thulaseedharan A (2007) Differential expression pattern of rubber elongation factor (REF) mRNA transcripts from high and low yielding clones of rubber tree (*Hevea brasiliensis* Muell. Arg.). Plant Cell Rep **26:** 1833–1838

Roux A, Cuvelier D, Nassoy P, Prost J, Bassereau P, Goud B (2005) Role of curvature and phase transition in lipid sorting and fission of membrane tubules. EMBO J **24:** 1537–1545

Santos Mendoza M, Dubreucq B, Miquel M, Caboche M, Lepiniec L (2005) LEAFY COTYLEDON 2 activation is sufficient to trigger the accumulation of oil and seed specific mRNAs in Arabidopsis leaves. FEBS Lett **579:** 4666–4670

Seo SG, Kim JS, Yang YS, Jun BK, Kang SW, Lee GP, Kim W, Kim JB, Lee HU, Kim SH (2010) Cloning and characterization of the new multiple stress responsible gene I (MuSI) from sweet potato. Genes Genomics **32:** 544–552

Shamas-Din A, Bindner S, Chi X, Leber B, Andrews DW, Fradin C (2015) Distinct lipid effects on tBid and Bim activation of membrane permeabilization by pro-apoptotic Bax. Biochem J **467:** 495–505

Shimada TL, Hara-Nishimura I (2015) Leaf oil bodies are subcellular factories producing antifungal oxylipins. Curr Opin Plant Biol **25:** 145–150

Shimada TL, Takano Y, Hara-Nishimura I (2015) Oil body-mediated defense against fungi: from tissues to ecology. Plant Signal Behav **10:** e989036

Shimada TL, Takano Y, Shimada T, Fujiwara M, Fukao Y, Mori M, Okazaki Y, Saito K, Sasaki R, Aoki K, et al (2014) Leaf oil body functions as a subcellular factory for the production of a phytoalexin in Arabidopsis. Plant Physiol **164:** 105–118

Shockey JM, Gidda SK, Chapital DC, Kuan JC, Dhanoa PK, Bland JM, Rothstein SJ, Mullen RT, Dyer JM (2006) Tung tree DGAT1 and DGAT2 have nonredundant functions in triacylglycerol biosynthesis and are localized to different subdomains of the endoplasmic reticulum. Plant Cell **18:** 2294–2313

Siloto RM, Findlay K, Lopez-Villalobos A, Yeung EC, Nykiforuk CL, Moloney MM (2006) The accumulation of oleosins determines the size of seed oilbodies in *Arabidopsis*. Plant Cell **18:** 1961–1974

Sookmark U, Pujade-Renaud V, Chrestin H, Lacote R, Naiyanetr C, Seguin M, Romruensukharom P, Narangajavana J (2002) Characterization of polypeptides accumulated in the latex cytosol of rubber trees affected by the tapping panel dryness syndrome. Plant Cell Physiol **43:** 1323–1333

Stitt M, Zeeman SC (2012) Starch turnover: pathways, regulation and role in growth. Curr Opin Plant Biol **15:** 282–292

Szymanski KM, Binns D, Bartz R, Grishin NV, Li WP, Agarwal AK, Garg A, Anderson RG, Goodman JM (2007) The lipodystrophy protein seipin is found at endoplasmic reticulum lipid droplet junctions and is important for droplet morphology. Proc Natl Acad Sci USA **104:** 20890–20895

Tarazona P, Feussner K, Feussner I (2015) An enhanced plant lipidomics method based on multiplexed liquid chromatography-mass spectrometry reveals additional insights into cold- and drought-induced membrane remodeling. Plant J **84:** 621–633

Tsai CH, Zienkiewicz K, Amstutz CL, Brink BG, Warakanont J, Roston R, Benning C (2015) Dynamics of protein and polar lipid recruitment during lipid droplet assembly in *Chlamydomonas reinhardtii*. Plant J **83:** 650–660

Vanhercke T, El Tahchy A, Liu Q, Zhou XR, Shrestha P, Divi UK, Ral JP, Mansour MP, Nichols PD, James CN, et al (2014) Metabolic engineering of biomass for high energy density: oilseed-like triacylglycerol yields from plant leaves. Plant Biotechnol J **12:** 231–239

van Rooijen GJ, Moloney MM (1995) Structural requirements of oleosin domains for subcellular targeting to the oil body. Plant Physiol **109:** 1353–1361

Wagner S, Bader ML, Drew D, de Gier JW (2006) Rationalizing membrane protein overexpression. Trends Biotechnol **24:** 364–371

Weise SE, Aung K, Jarou ZJ, Mehrshahi P, Li Z, Hardy AC, Carr DJ, Sharkey TD (2012) Engineering starch accumulation by manipulation of phosphate metabolism of starch. Plant Biotechnol J **10:** 545–554

Winter D, Vinegar B, Nahal H, Ammar R, Wilson GV, Provart NJ (2007) An "Electronic Fluorescent Pictograph" browser for exploring and analyzing large-scale biological data sets. PLoS ONE **2:** e718

Wolvetang EJ, Tager JM, Wanders RJ (1990) Latency of the peroxisomal enzyme acyl-CoA:dihydroxyacetonephosphate acyltransferase in digitonin-permeabilized fibroblasts: the effect of ATP and ATPase inhibitors. Biochem Biophys Res Commun **170:** 1135–1143

Yang H, Galea A, Sytnyk V, Crossley M (2012a) Controlling the size of lipid droplets: lipid and protein factors. Curr Opin Cell Biol **24:** 509–516

Yang HJ, Hsu CL, Yang JY, Yang WY (2012b) Monodansylpentane as a blue-fluorescent lipid-droplet marker for multi-color live-cell imaging. PLoS ONE **7:** e32693

Zale J, Jung JH, Kim JY, Pathak B, Karan R, Liu H, Chen X, Wu H, Candreva J, Zhai Z, et al (2016) Metabolic engineering of sugarcane to accumulate energy-dense triacylglycerols in vegetative biomass. Plant Biotechnol J **14:** 661–669